Pure appl. geophys. 162 (2005) 1151–1185
0033–4553/05/071151-35
DOI 10.1007/s00024-004-2665-4

© Birkhäuser Verlag, Basel, 2005

Pure and Applied Geophysics

Methods for Measuring Seismicity Rate Changes: A Review and a Study of How the M_w 7.3 Landers Earthquake Affected the Aftershock Sequence of the M_w 6.1 Joshua Tree Earthquake

David Marsan[1] and Suleyman S. Nalbant[2]

Abstract—The development of fault interaction models has triggered the need for an accurate estimation of seismicity rate changes following the occurrence of an earthquake. Several statistical methods have been developed in the past to serve this purpose, each relying on different assumptions (e.g., stationarity, gaussianity) pertaining to the seismicity process.

In this paper we review these various approaches, discuss their limitations, and propose further improvements. The feasibility of mapping robust seismicity rate changes, and more particularly rate decreases (i.e., seismicity shadows), in the first few days of an aftershock sequence, is examined. To this aim, the hypothesis of large numbers of earthquakes, hence the use of Gaussian statistics, as is usually assumed, must be dropped.

Finally, we analyse the modulation in seismicity rates following the 1992, June 28 M_w 7.3 Landers earthquake in the region of the 1992, April 22 M_w 6.1 Joshua Tree earthquake. Clear instances of early triggering (i.e., in the first few days) followed by a seismicity quiescence, are observed. This could indicate the existence of two distinct interaction regimes, a first one caused by the destabilisation of active faults by the travelling seismic waves, and a second one due to the remaining static stress perturbation.

Key words: Seismology, fault interactions, seismic quiescence.

1. The Need for Estimating Reliable Seismicity Rates

The recent development of fault interaction models has underlined the practical need for statistical estimations of seismicity rates. Of particular importance is the question of how such rates evolve with time, as for example following the stress redistribution caused by the occurrence of an earthquake. Only with the systematic comparison between model predictions and the actual seismicity dynamics, as observed through such rate estimates, can further progress be made towards a global understanding of what are the significant processes (and their associated time scales) at work in fault interactions.

[1] Laboratoire de Géophysique Interne et Tectonophysique, Université de Savoie, 73376 Le Bourget du Lac, France. E-mail: david.marsan@univ-savoie.fr

[2] Geophysics Research Group, University of Ulster, Coleraine, Co. Derry, BT52 1SA, Northern Ireland. E-mail: ss.nalbant@ulster.ac.uk

A timely example is provided by the question surrounding seismicity shadows, and their relation to dynamic stress triggering. Their absence, as argued by FELZER *et al.* (2003), could be seen as a proof that dynamic stress triggering controls most of the seismicity changes at all time scales. Observation of aftershocks occurring very early—e.g., up to days—in the aftershock sequence (see section 3), in zones modeled as static stress shadows and that indeed experience a slowing down of the seismicity at longer time scales, can be interpreted as due to a regime of dynamic triggering that acts on the most unstable faults (VOISIN *et al.*, 2004). The slip-dependent friction model of VOISIN *et al.* (2000), applied to the 1980 Irpinia sequence, and the rate-and-state friction model studied by BELARDINELLI *et al.* (2003), both predict that the time scale of such triggering is short, so that the two regimes of dynamic and static triggering can be distinguished in time. Although seismicity shadows are indeed uncommon, as observed in the first year following the 1989 Loma Prieta, the 1992 Landers and the 1994 Northridge earthquakes (MARSAN, 2003), instances of rate decreases coincident with the occurrence of a main shock have been documented by TODA and STEIN (2003) and WOESSNER *et al.* (2004), in the case of the 1997 Kagoshima sequence, prompting the claim that dynamic triggering might not be significant (TODA and STEIN, 2003) in modulating the local pattern of seismicity. That such diverging conclusions have been reached in recent years shows the need for developing a common statistical framework designed to detect seismicity shadows, along with an estimate of their life-time. A general consensus on such a method has yet to be reached.

More generally, a key issue in fault interaction modelling is the relation between stress changes and seismicity dynamics. The comparison of a relation, as for example stemming from laboratory-based friction models, against actual earthquake population dynamics (TODA *et al.*, 1998; DIETERICH *et al.*, 2000; TODA and STEIN, 2003), requires that the latter is rigorously described. In particular, statistical measures of the seismicity changes and their significance (i.e., whether they are anomalous or could be due to pure luck) necessitate the use of a null hypothesis regarding the seismicity dynamics that properly accounts for its non-stationarity.

The present paper aims at describing previous efforts in developing such a method (section 2). The case of the seismicity changes following the 1992 Landers earthquake in the epicentral zone of the 1992 Joshua Tree earthquake will serve as an illustration (section 3).

2. Methods for Measuring Seismicity Rate Changes

2.1 General Framework

The general framework for estimating seismicity rate changes can be formalised as follows (cf. Fig. 1):

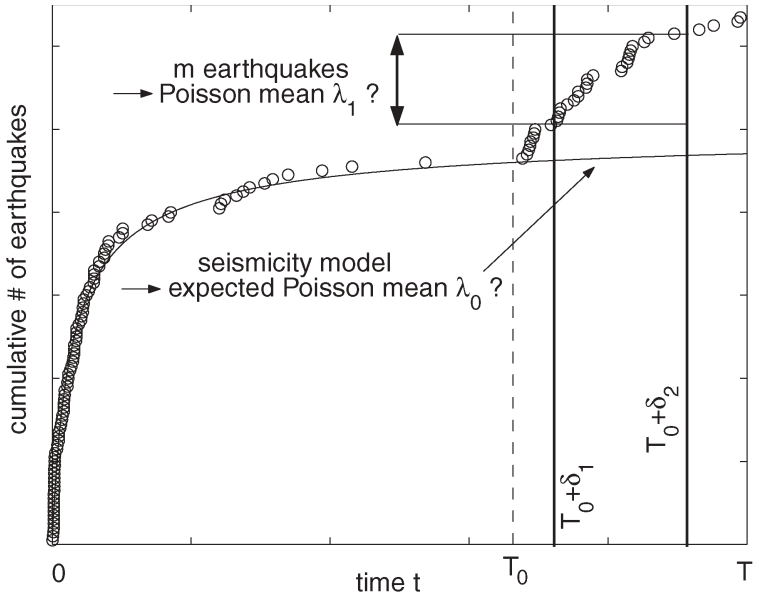

Figure 1
The seismicity change occurring between $T_0 + \delta_1$ and $T_0 + \delta_2$ is estimated by comparing the Poisson mean λ_1, such that the number m of earthquakes actually occurring in the time interval is a realisation of a Poisson distribution with mean λ_1, with the expected Poisson mean λ_0 that would be predicted by a seismicity model if the seismicity time series was only known up to time T_0.

1. Given a crustal volume V;
2. Knowing $\{t_i\}$ the times of occurrences of the earthquakes in V between time 0 and time T;
3. How can we estimate the earthquake occurrence rate λ_1, in the time interval $[T_0 + \delta_1, T_0 + \delta_2]$, with $0 < T_0 + \delta_1 < T_0 + \delta_2 < T$?
4. And how 'anomalous' is this estimated rate compared to the expected rate λ_0, in relation to the occurrence of a particular event (e.g., a large earthquake) at time T_0 (see below for more explanations)?

Items 3 and 4 require the description of earthquake occurrence in terms of a Poisson temporal process, i.e., an infinitely divisible stochastic process such that the number of earthquakes in any interval $[t, t + \delta]$ follows a Poisson distribution with mean

$$\lambda(t, t + \delta) = \int_t^{t+\delta} ds\, \lambda(s). \tag{1}$$

This process is fully described by the mean rate $\lambda(t)$ defined on the interval $[0, T]$. A crucial aspect is that the observed earthquake times $\{t_i\}$ are only realisations of

the Poisson process defined by the mean rate λ on the interval $[0, T]$: The unknown is the Poisson mean $\lambda_1 = \lambda(T_0 + \delta_1, T_0 + \delta_2)$, which can only be estimated from the observed times $\{t_i\}$. The number m of earthquakes in $[T_0 + \delta_1, T_0 + \delta_2]$ is then a realisation of the Poisson distribution $P(m) = \exp(-\lambda_1)\lambda_1^{m!}/m!$. It is therefore expected that item 3 results in a *distribution* of the estimate $\hat{\lambda}_1$ of the unknown λ_1, hence a probability density function, or pdf, $f_1\left(\hat{\lambda}_1\right)$. This important point is sometimes overlooked, leading to claims that the sample rate $m/(\delta_2 - \delta_1)$ is *the* seismicity rate of interest while m is only a realisation of the actual Poisson random variable with mean λ_1, which can only be known through an estimate $\hat{\lambda}_1$ and its pdf $f_1\left(\hat{\lambda}_1\right)$.

Item 4 is certainly the most difficult to address, and is at present what limits our ability to propose a general and unambiguous method. When estimating a change in the seismicity rate, related to the occurrence of an earthquake at time T_0, we need to know what distribution should follow the Poisson mean λ_0 in $[T_0 + \delta_1, T_0 + \delta_2]$ if the seismicity had not been perturbed at T_0. This can be done by assuming that the seismicity is only known up to T_0, and then by modelling, i.e., extrapolating, the expected mean λ_0 between $T_0 + \delta_1$ and $T_0 + \delta_2$. This comparison between the estimates $\hat{\lambda}_1$ and $\hat{\lambda}_0$ of the actual mean λ_1 and of the expected mean λ_0, respectively, will allow us to estimate whether a significant change in seismicity has been experienced by the crustal volume V. In order to estimate the pdf of $\hat{\lambda}_0$, a model for the seismicity process $\lambda(t)$ knowing $\{t_i < T_0\}$ is required. This procedure is equivalent to transforming the non-stationary seismicity point-process $\{t_i\}$ into a stationary process $\{\tau_i\}$ such that $t_i \to \tau_i = \lambda(0, t_i) = \int_0^{t_i} ds\, \lambda(s)$, e.g., the residual analysis of OGATA (1988).

In the next two sections, we discuss the various methods used to implement items 3 and 4, and more particularly (1) how the distribution of the expected (predicted) mean rate $\hat{\lambda}_0$ can be estimated, and (2) how the change in seismicity and its significance can be measured, as the departure of the pdf of $\hat{\lambda}_1$ (Poisson mean conditioned by the observed $\{T_0 + \delta_1 < t_i < T_0 + \delta_2\}$) from the pdf of $\hat{\lambda}_0$ (expected Poisson mean deduced from the seismicity model, conditioned by the observed $\{0 < t_i < T_0\}$).

2.2 Seismicity Models and Prediction of the Poisson Mean λ_0 (Null Hypothesis)

A probabilistic model of earthquake occurrence must be proposed, that is only conditioned by the occurrence times $\{t_i < T_0\}$ (and possibly by other source parameters like the magnitude), in order to estimate what a normal rate of occurrence should be during $[T_0 + \delta_1, T_0 + \delta_2]$. This corresponds to building a null hypothesis against which the real seismicity process in $[T_0 + \delta_1, T_0 + \delta_2]$ must be tested. The fact that changes in the choice of the null hypothesis can lead to significant changes in the seismicity estimates is a testimony of the difficulty of selecting a suitable model.

Many point-process models of seismicity have been proposed, see VERE-JONES (1992) and OGATA (1999) for reviews. It is not intended here to give an extensive review of these models, but rather to describe the ones that have been used in order to compute seismicity rate changes following large earthquakes. No consensus exists at present as to which model one should systematically resort to for the present purpose. MATTHEWS and REASENBERG (1988) and associated further work (REASENBERG and MATTHEWS, 1988; REASENBERG and SIMPSON, 1992; KILB *et al*., 2000; GOMBERG *et al*., 2001; along with WYSS and WIEMER, 2000) used the declustering algorithm of REASENBERG (1985) to only preserve the part ('background' seismicity) of seismicity considered as being devoid of aftershocks. Such a type of construction is not pertinent to the present problem (OGATA, 1992; MARSAN, 2003), most particularly because the aftershocks triggered by the earthquake that occurred at T_0 are clearly of paramount importance when estimating whether a region has undergone a positive or a negative rate change. Aftershocks need to be kept rather than discarded.

The simplest approach was followed by TODA *et al*. (1998, 2002) and TODA and STEIN (2003) who assumed stationarity of the process, so that a well-defined background rate can be estimated from past seismicity, and compared to the rate of aftershock production. This should generally be avoided, as any long-lasting seismicity trends, such as previous aftershock sequences still ongoing at the time of the main shock occurrence, will contaminate these estimates. This typically leads to a systematic underestimation of the rate change (MARSAN, 2003; FELZER *et al*., 2003). Also, the choice of the time interval for calculating the *a priori* (background) rate is arbitrary.

WOESSNER *et al*. (2004) analysed the changes caused by the 2nd main shock of the 1997 Kagoshima sequence on the seismicity pattern triggered by the 1st main shock. They modeled the evolution of this early seismicity using the modified Omori-Utsu law (UTSU, 1961), and added complexity to this model by embedding secondary aftershock sequences when felt necessary (UTSU, 1970; see also OGATA and SHIMAZAKI, 1984, who modeled the aftershock sequence of the 1965 Rat Islands earthquake using a double Omori-Utsu law). They systematically tested for the goodness of fit using a Kolmogorov-Smirnov test.

MARSAN (2003) tested several models: (a) an autoregressive model, which proved not to be well adapted to this specific task as it systematically overestimates the future rate during rate-decaying aftershock sequences; (b) a sum of N power-laws (UTSU, 1970), which generalizes the model of OGATA and SHIMAZAKI (1984) and WOESSNER *et al*. (2004); (c) the ETAS model (OGATA, 1988), both in its continuous and discrete forms, the latter being much less computationally expensive than the former. The ETAS model is a linear Poisson process that fully develops the embedded cascade of secondary, tertiary, ..., aftershocks. While it certainly is a very good model for the present purpose of predicting an unperturbed seismicity state, its numerical treatment can raise some practical difficulties. Inversion of its parameters is not robust, and

frequently yields unstable models (i.e., models characterised by a branching ratio —or mean number of earthquakes triggered by an earthquake— greater than one). Also, this inversion and the subsequent Monte-Carlo simulations (see section 2) required to estimate the pdf of $\hat{\lambda}_0$ (predicted Poisson mean) can be computationally onerous, the more so when this procedure is iterated to many grid cells. Finally, it is assumed in this model that the onsets of the power-law decaying rate changes must coincide with the occurrence of earthquakes reported in the analysed catalogue. The fluctuations in seismicity in any given cell/region caused by an earthquake located outside it are therefore badly modeled. An improvement would consist in considering space-time ETAS models (see VERE-JONES, 1992, and OGATA, 1999, for reviews). However, even the simplest, not to say simplistic, isotropic space-time kernels require an even longer and less robust inversion of the model parameters.

The ETAS model was developed and used by OGATA (1988, 1992) and OGATA *et al.* (2003) to detect anomalous quiescences preceding or following large earthquakes. Distinct parameter sets of the model over distinct time intervals can be obtained, according to a selection criterion. As mentioned previously, the residual analysis performed in these studies consists in transforming the nonstationary Poisson process $\{t_i\}$ into a stationary one $\{\tau_i\}$. Deviations from stationarity of this transformed process $\{\tau_i\}$ are then searched for. A particularity with the work of OGATA (1988, 1992) and OGATA *et al.* (2003), compared to the one proposed here, is that the best fitting model was estimated for the complete time interval $[0, T]$ rather than on the a priori interval $[0, T_0]$. Normality has then a stronger sense: if the earthquake occurring at time T_0 triggers numerous aftershocks of which decaying rate is well modeled by the best-fitting model, then no anomalous behaviour is reported. The present manuscript rather attempts to detail the changes in seismicity that follow this earthquake, with no *a priori* knowledge of its occurrence.

2.3 Statistical Measures

In their pioneering work, MATTHEWS and REASENBERG (1988) developed a sound and rigorous statistical framework for detecting seismicity patterns, even though they accounted for the nonstationarity of the process by using the declustering algorithm of REASENBERG (1985). While this method was primarily intended to analyse precursory seismic quiescences (REASENBERG and MATTHEWS, 1988), it can equally be applied to estimating seismicity changes following main shocks (REASENBERG and SIMPSON, 1992; KILB *et al.*, 2000; GOMBERG *et al.*, 2001). They introduced the β statistic, as a measure of the significance of the departure from stationarity in the seismogenic process (i.e., their null hypothesis after the catalogue has been declustered is that the remaining 'background' seismicity is stationary), along with a maximum likelihood estimate $\hat{\rho}$ of the rate ratio itself. Given that n earthquakes occurred in the total time of observation $[0, T]$, the number $m \leq n$ of earthquakes falling in the interval $[T_0 + \delta_1, T_0 + \delta_2]$ follows a binomial distribution. This micro-canonical view

(fixed total number n of earthquakes) can easily be extended to the more pertinent canonical framework where the average number of events in the observation time rather than the realised number is fixed. Recast in the same notations as section 2.1, the expected number of earthquakes that should occur in $[T_0 + \delta_1, T_0 + \delta_2]$ follows a Poisson distribution with mean λ_0 and standard deviation $\sqrt{\lambda_0}$, so that a departure of the observed number m from λ_0 becomes significant when it is higher than $\sqrt{\lambda_0}$. Here the distribution of $\hat{\lambda}_1$ is taken as concentrated on m, which is the maximum likelihood estimator (see below for a more complete construction): $f_1\left(\hat{\lambda}_1\right) = \delta\left(m - \hat{\lambda}_1\right)$, where $\delta(.)$ is the generalised Dirac function. The statistic β can therefore be redefined as

$$\beta = \frac{m - \lambda_0}{\sqrt{\lambda_0}}. \tag{2}$$

Note that the seismicity model yields a pdf f_0 for the estimate $\hat{\lambda}_0$ of λ_0, so that this relation should rather be integrated over this pdf:

$$\beta = \int_0^\infty d\hat{\lambda}_0 \, f_0\left(\hat{\lambda}_0\right) \frac{m - \hat{\lambda}_0}{\sqrt{\hat{\lambda}_0}}. \tag{3}$$

The development of MATTHEWS and REASENBERG (1988) is further based on assuming large numbers n and m of events, which allows to approximate m, and hence β itself, as normal random variables. Unfortunately, this assumption needs to be relaxed when considering small or weakly active crustal volumes and short durations of observation. Such an extension was done in MARSAN (2003), with the definition of two measures: the probability of triggering $\mathscr{P}$ and the mean logarithm $E\{\log \hat{r}\}$ of the rate ratio estimate $\hat{r} = \hat{\lambda}_1/\hat{\lambda}_0$, in place of β and $\hat{\rho}$ of MATTHEWS and REASENBERG (1988). Knowing that m earthquakes occurred in $[T_0 + \delta_1, T_0 + \delta_2]$, the likelihood f_1 of the mean $\hat{\lambda}_1$ is

$$f_1\left(\hat{\lambda}_1\right) = e^{-\hat{\lambda}_1} \frac{\hat{\lambda}_1^m}{m!}. \tag{4}$$

The probability that the interval $[T_0 + \delta_1, T_0 + \delta_2]$ has experienced a positive change in seismicity is given by

$$\mathscr{P} = \text{ probability that } \hat{\lambda}_1 > \hat{\lambda}_0 \tag{5}$$

$$= \int_0^\infty d\hat{\lambda}_0 \, f_0\left(\hat{\lambda}_0\right) \int_{\hat{\lambda}_0}^\infty d\hat{\lambda}_1 \, f_1\left(\hat{\lambda}_1\right) \tag{6}$$

which, along with equation (4), yields

$$\mathscr{P} = 1 - \int_0^\infty d\hat{\lambda}_0 \, f_0\left(\hat{\lambda}_0\right) P\left(m + 1, \hat{\lambda}_0\right), \tag{7}$$

where P is the incomplete Gamma function (see MARSAN, 2003). In the null hypothesis that the distributions of $\hat{\lambda}_1$ and $\hat{\lambda}_0$ are the same, $\mathscr{P}$ is a uniform random variable on $[0, 1]$, so that the condition $\mathscr{P} < \epsilon$ or $\mathscr{P} > 1 - \epsilon$ should only occur with probability 2ϵ. A significant change in rate would for example be given by $\epsilon = 10^{-3}$ or less (99.9% significance), i.e., it would take on average 10^3 random realisations of the null hypothesis to see one such $\mathscr{P}$ occurring by chance. A more readable measure is given by

$$\gamma = -\text{sign } (\mathscr{P} - 1/2) \times \log_{10}(\min\{\mathscr{P}, 1 - \mathscr{P}\}). \tag{8}$$

If $\mathscr{P} = 10^{-3}$, then $\gamma = -3$, hence indicating a (99.9%) significant rate decrease, while if $\mathscr{P} = 1 - 10^{-3}$, then $\gamma = +3$, i.e., a (99.9%) significant rate increase. An estimate of the ratio of the change in rates is given by

$$E\left\{\log_{10}\frac{\hat{\lambda}_1}{\hat{\lambda}_0}\right\} = \int_0^\infty d\hat{\lambda}_1 f_1\left(\hat{\lambda}_1\right) \log \hat{\lambda}_1 - \int_0^\infty d\hat{\lambda}_0 f_0\left(\hat{\lambda}_0\right) \log \hat{\lambda}_0. \tag{9}$$

In the limit of very large numbers of earthquakes, these statistics are equivalent to the ones of MATTHEWS and REASENBERG (1988).

Another measure of the significance of the change in seismicity rate was proposed by HABERMANN (1983), and used by WYSS and WIEMER (2000) to estimate the triggering and quiescence patterns following the 1992 Landers earthquake. The statistic Z is a classical measure for testing whether two independent populations have the same mean or not. In the present context, we need to discretize the time axis in time bins of length δ; the two intervals $[0, T_0]$ and $[T_0 + \delta_1, T_0 + \delta_2]$ have $N_0 = T_0/\delta$ and $N_1 = \Delta/\delta$ such bins, with $\Delta = \delta_2 - \delta_1$, respectively. If the numbers of earthquakes $\left\{m_0^{(1)}, m_0^{(2)}, \ldots, m_0^{(N_0)}\right\}$ and $\left\{m_1^{(1)}, m_1^{(2)}, \ldots, m_1^{(N_1)}\right\}$ are all independent realisations of the two independent random variables m_0 and m_1 with mean λ_0 and λ_1 and standard deviations σ_0 and σ_1 respectively, then the sample means $\mu_0 = \frac{1}{N_0}\left(m_0^{(1)} + m_0^{(2)} + \cdots + m_0^{(N_0)}\right)$ and $\mu_1 = \frac{1}{N_1}\left(m_1^{(1)} + m_1^{(2)} + \cdots + m_1^{(N_1)}\right)$ converge towards two independent normal random variables $\mathscr{N}\left(\lambda_0, \sigma_0'\right)$ and $\mathscr{N}\left(\lambda_1, \sigma_1'\right)$ with standard deviations $\sigma_0' = \sigma_0/\sqrt{N_0}$ and $\sigma_1' = \sigma_1/\sqrt{N_1}$. The difference $\mu_1 - \mu_0$ is then distributed according to $\mathscr{N}(\lambda_1 - \lambda_0, \sigma)$ with $\sigma^2 = \sigma_0'^2 + \sigma_1'^2 = \frac{\sigma_0^2}{N_0} + \frac{\sigma_1^2}{N_1}$. The random variable $Z = \frac{\mu_1 - \mu_0}{\sigma}$ therefore follows a $\mathscr{N}\left(\frac{\lambda_1 - \lambda_0}{\sigma}, 1\right)$ distribution. To test whether λ_1 significantly departs from λ_0, Z is computed and compared to $\mathscr{N}(0, 1)$, which characterizes its distribution if $\lambda_0 = \lambda_1$. Note that, given the assumption of independence of the process, m_0 and m_1 are Poisson random variables, which leads to redefining Z as

$$Z = \frac{m\frac{T_0}{\Delta} - n_0}{\sqrt{n_0 + m\frac{T_0^2}{\Delta^2}}} \tag{10}$$

with n_0 and m being the number of earthquakes in $[0, T_0]$ and $[T_0 + \delta_1, T_0 + \delta_2]$. This statistic strongly resembles the β statistic of equation (2), apart from the symmetric

role now played by the *a priori* n_0 and observed m numbers in defining the standard deviation in the denominator. Like β, the statistic Z relies on approximating Poisson distribution with normal distributions, which requires large numbers of earthquakes; it is therefore not well adapted to a fine scale mapping of seismicity changes at short time scales.

Finally, OGATA (1988) proposed the use of a method by SHIMIZU and YUASA (1984) that transforms a Poisson law into a random variable well approximated by a centered unit normal distribution $\mathcal{N}(0,1)$. Departures from the expected Poisson distribution are then documented with significance levels given in unit standard deviations.

2.4 The Special Case of Seismicity Shadows

As discussed in section 1, seismicity shadows have been reported to be difficult to observe (MARSAN, 2003) or even to be missing (FELZER *et al.*, 2003; MALLMAN and ZOBACK, 2003), for several instances of recent $M6$ to M 7.3 earthquakes in California. Before embarking on such an analysis, it has first to be noted that a seismicity shadow, i.e., a decrease in the seismicity rate at $t > T_0$, can go undetected if the crustal volume V under scrutinity is too small, or if the time of observation is too short. Both conditions can lead to a small expected rate λ_0, in which case the analysis is very strongly biased towards triggering.

To illustrate this, consider a case where only $\lambda_0 = 2$ earthquakes / year are expected (on average) to occur in V in the time interval $[T_0 + \delta_1, T_0 + \delta_2]$. It will then take approximately 6 months of observation to ascertain that earthquakes are missing, if V has indeed been subjected to a complete shutdown of its seismicity; this duration increases to 2.4 years if a 99% significance level is required, see below. On the other hand, if V undergoes an enhancement of its seismicity rate, this triggering will be detected unambiguously for much shorter observation durations. As an example, an increase will be reported to exist at the 99% significance level, with no ambiguity, after about 1 to 2 days if the seismicity is increased by a factor $r = 100$, see Figure 2.

Figure 2 (see also the Appendix) gives the ensemble-averaged γ value of equation (8) and $E\{\log_{10}\hat{r}\}$ of equation (9), vs. the duration $\Delta = \delta_2 - \delta_1$ of observation, in the case $f_0\left(\hat{\lambda}_0\right) = \delta\left(\hat{\lambda}_0 - 2\right)$, i.e., $\hat{\lambda}_0$ is concentrated on 2 earthquakes / unit time ($\delta(.)$ being the generalised Dirac function), and for several cases of seismicity change. In the most extreme case of a total shutdown of the seismicity (yielding values of $E\{\log_{10}\hat{r}\}$ and γ very close to the ones for $r = 0.01$ of Figure 2, for $0 < \Delta \leq 10$ years), the first $\simeq 3.6$ months will, on ensemble average, be reported as showing an increase of seismicity. The significance of this increase will even be high ($\gamma > 2$, hence a 99% significance level) for the first $\simeq 1.8$ days. A seismicity shadow will only be reported with a 99% significance or better for $\Delta > 2.4$ years. At $\Delta = 2.4$ years, the estimated mean of the log-ratio $E\{\log_{10}\hat{r}\}$ is found to be $\simeq -0.93$, instead of the expected -2. Figure 3 shows the two measures $E\{\log_{10}\hat{r}\}$ and γ at this time scale of $\Delta = 2.4$ years,

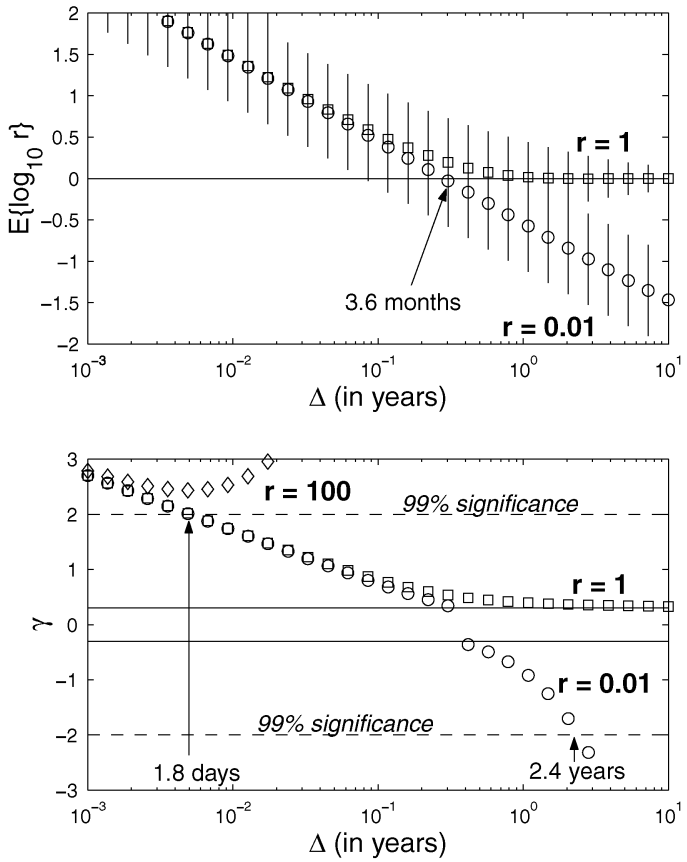

Figure 2

$E\{\log_{10}\hat{r}\}$ (top graph) and γ (bottom graph) vs. observation duration Δ in years, for $r = 100$ ($\diamond$), $r = 1$ ($\square$) and $r = 0.01$ ($\circ$), and $\lambda_0 = 2$ earthquakes/year. For $r = 100$, $E\{\log_{10}\hat{r}\} > 2$ for $0 < \Delta \leq 10$ years. The 99% significance levels are indicated for γ (dashed lines), along with the two values $\log_{10} 0.5$ and $-\log_{10} 0.5$ (continuous lines) between which γ is excluded by construction, see equation (8). The vertical error bars in the top graph have a length that is twice the standard deviation of $\log_{10}\hat{r}$.

for a varying rate change ratio r. A correct estimate of r is obtained after $\Delta = 2.4$ years for r roughly above 10^{-1} (Fig. 3, top graph), but with a low significance ($\gamma \simeq -1.5$ for $r = 10^{-1}$). In all cases, $E\{\log_{10}\hat{r}\}$ eventually converges to the correct value $\log_{10} r$, as $t \to \infty$, with γ going to plus or minus infinity. This case $t \to \infty$ of very large numbers of earthquakes is essentially the one treated by MATTHEWS and REASENBERG (1988).

As illustrated in this example, there exists a minimum duration of observation required, on ensemble average, in order to observe a seismicity shadow at a given (high) significance level. This is also true for unambiguously detecting triggering, but it implies shorter durations for a similar level of significance: at very short time scales,

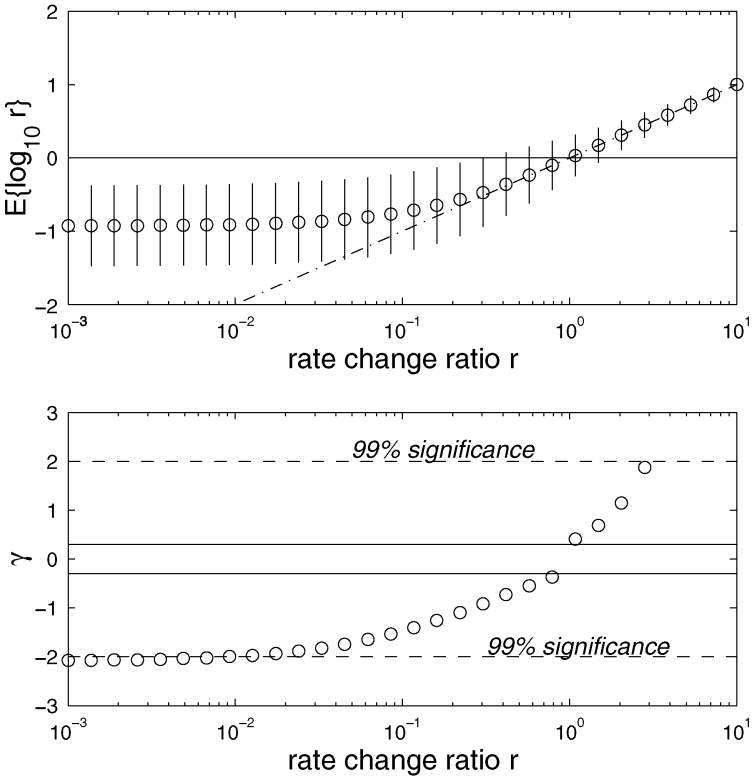

Figure 3
$E\{\log_{10}\hat{r}\}$ (top graph) and γ (bottom graph) vs. rate change ratio r at $\Delta = 2.4$ years, for $\lambda_0 = 2$ earthquakes/year. The estimator $E\{\log_{10}\hat{r}\}$ yields correct values of r (dash-dotted line, top graph) for ratio r greater than about 10^{-1}. The 99% significance levels are indicated for γ (dashed lines). The vertical error bars in the top graph have twice the length of the standard deviation of $\log_{10}\hat{r}$.

there is no possibility of distinguishing between various values of r, hence a low resolution of the method and the ambiguity on the actual seismicity rate change. This asymmetry between triggering and quiescence can lead to the spurious observation of triggering in regions actually experiencing a slowing down of their seismicity. MARSAN (2003) proposed a correction to the method in order to unbias $E\{\log_{10}\hat{r}\}$ (see Appendix A of MARSAN, 2003). However, this correction is only possible for time scales of the order of $1/\lambda_0$, and the gain in accurracy obtained by introducing it is therefore limited to the transition regime between undetectability and detectability of the seismicity shadow.

A solution to this problem is to make sure that λ_0 is large enough, either by increasing the size of the region V, or by adjusting the duration of observation. The former approach was taken by WYSS and WIEMER (2000), and the second by FELZER *et al.* (2003). In the first case, other issues can arise when the crustal volume V is

composed of two subvolumes V_A and V_B subjected to triggering and quiescence, respectively. This can typically be the case when V probes the fault (or its proximity) that slipped at time T_0, or when V is too large compared to the rupture length of the earthquake that occurred at T_0. A simple handwaving argument indicates that if V_A and V_B both have an expected number of say 10 earthquakes for the observation duration Δ, and that V_A experiences a $r_A = 10^2$ increase and V_B a $r_B = 10^{-2}$ decrease of their seismicity, then, assuming independence of the two subvolumes V_A and V_B, the overall volume $V = V_A + V_B$ is characterised by a rate change ratio r of the order of $\frac{10\times 10^2 + 10\times 10^{-2}}{10+10} = 50$, hence a strong triggering. A more careful estimate, based on the development of section 3, gives that, on ensemble average, $E\{\log_{10}\hat{r}\} = 1.70$ which is equal to $\log_{10} 50$ with a very good precision, along with $\gamma > 14$ (resolution limit of the floating type of the mathematical software used). This asymmetry comes from the nonlinearity of the logarithm of the rate change ratio $\log r$ with the logarithm of the rate change: $\log r = \log \frac{\lambda_0 r_A + \lambda_0 r_B}{2\lambda_0} = \log \frac{r_A + r_B}{2}$ is not equal to the mean $\frac{1}{2}[\log r_A + \log r_B]$.

Seismicity shadows will therefore go unnoticed if their spatial extent is smaller than the resolution scale of the grid (while seismicity triggers will not). It then becomes a problem to choose circular regions with a radius adjusted so that the expected rate λ_0 becomes large enough, as is sometimes done (e.g., WYSS and WIEMER, 2000). If the objective of the analysis is to detect seismicity shadows, then a more appropriate procedure for selecting the shape and the size of the region must be adopted. This will be attempted in section 5.

FELZER *et al.* (2003) estimated the rate change ratio $\hat{r} = t_0/t_1$ by comparing the time t_1 it takes for the first N earthquakes to occur immediately after T_0, to the time t_0 for the last N earthquakes to occur prior to T_0, with $N = 5$ or less. The mean log-ratio $E\{\log\hat{r}\}$ is then no longer bounded in the $E\{\log\hat{r}\} \gg 1$ or the $E\{\log\hat{r}\} \ll -1$ directions. The significance, or probability of triggering defined in equation (7), then becomes

$$\mathscr{P} = \int_0^\infty d\hat{\lambda}_0 \, \frac{\hat{\lambda}_0 t_0^2}{N^2} \, e^{-\hat{\lambda}_0 t_0/N} \int_{\hat{\lambda}_0}^\infty d\hat{\lambda}_1 \, \frac{\hat{\lambda}_1 t_1^2}{N^2} \, e^{-\hat{\lambda}_1 t_1/N} \tag{11}$$

$$= \frac{\hat{r}^2(\hat{r}+3)}{(\hat{r}+1)^3} \tag{12}$$

still with $\hat{r} = t_0/t_1$. This probability can become very close to 0 or 1 independently of the number N. This method is however done at the cost of possibly very different time scales of observation from one place to the other. Also, it is very sensitive to the increase in the magnitude of completness immediately following a large earthquake. In order to test the significance of the seismicity shadows, FELZER *et al.* (2003) proposed comparison of the number of shadow occurrences following the time T_0 of interest to the number obtained at any random date.

Practically, the limit of detectability of seismicity shadows should be determined in the first place when analysing seismicity rate changes. In order to do so, given Δ, $f_0\left(\hat{\lambda}_0\right)$, and a minimum significance level γ_m:

- The maximum ratio $r_m < 1$ such that a shadow can be detected with $\gamma < \gamma_m$ is determined following the approach described in the Appendix.
- The bias on $E\{\log \hat{r}\}$ is specified for $r = r_m$.

In the case of Figure 3, for $\gamma_m = -2$ and $\Delta = 2.4$ years, this corresponds to $r_m \simeq 10^{-2}$ and a bias of $-0.93 + 2 = +1.07$ on the estimated logarithm of $\hat{r}$. This implies that, for an observation duration $\Delta = 2.4$ years of a zone with an expected rate of 2 earthquakes/year, 'mild' seismicity shadows characterised by rate change ratios between 10^{-2} and 1 will not be detected with sufficient significance, i.e., with a γ value less than -2, hence with significance level not better than 99%. For $r < 10^{-2}$, the 99% significance level is reached, however the estimated $E\{\log_{10} \hat{r}\}$ is too high by at least 1.07.

3. Analysis of the Seismicity Changes Caused by the 1992 Landers Earthquake in the Epicentral Zone of the 1992 Joshua Tree Earthquake

In this section we examine how the M_w 7.3 Landers earthquake changed the seismicity pattern in the zone of the M_w 6.1 Joshua Tree earthquake which occurred 66 days earlier. Because the Joshua Tree earthquake triggered a vigorous aftershock activity, any modulation by the Landers earthquake should be more easily detectable. Also, previous studies have reported seismicity shadows following the Landers earthquake (WYSS and WIEMER, 2000; MARSAN, 2003) that correlates well with modeled stress shadows (KING *et al.*, 1994; MCCLOSKEY *et al.*, 2003), east of the Joshua Tree rupture. The onset, duration, and general characteristics of this seismicity shadow can be investigated using the methodology of section 2.

3.1 Data

We use the SCSN catalogue (http://www.data.scec.org/ftp/catalogs/SCSN) with a completeness magnitude of $M = 2.2$, for both the time interval between the Joshua Tree and the Landers earthquakes, and the first year after the Landers earthquake. The zone studied is a 19 km $\times$ 39 km region defined by $-116.4^{\circ} \leq$ longitude $\leq -116.2^{\circ}$, and $33.85^{\circ} \leq$ latitude $\leq 34.2^{\circ}$, see Figure 4, and only the quality A, B and C earthquakes are kept. The error on epicentral location is 2 km and 5 km for quality B and C events, respectively.

The frequency-magnitude relationship appears to follow the Gutenberg-Richter law for $M \geq 2.2$, for the two time intervals between the Joshua Tree and the Landers earthquakes, and in the first year after the Landers earthquake. However, short time scale fluctuations of the completeness magnitude are known to exist, especially following large shocks (e.g., the Landers earthquake). As a result of the difficulty to

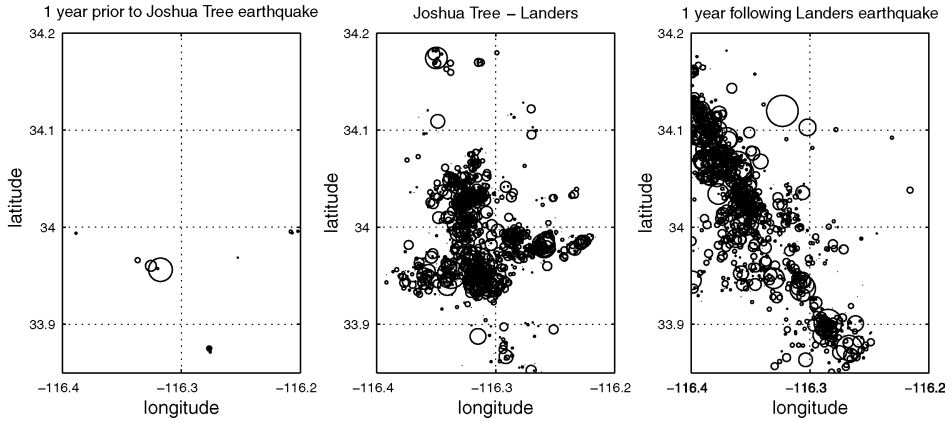

Figure 4
M 2.2+ earthquakes (left) in the year before the April 22, 1992 Joshua Tree earthquake, (center) in the 66 days between the Joshua Tree and the Landers earthquakes, and (right) in the year following the June 28, 1992 Landers earthquake, for the 19 km × 39 km region under study. The circles have sizes proportional to the magnitude.

single out individual aftershocks in the early stages of an aftershock sequence, many small *M* 2.2+ shocks are likely to be missed and absent of the catalogue. Figure 5 shows how the aftershocks of the Landers earthquake distribute over time in the

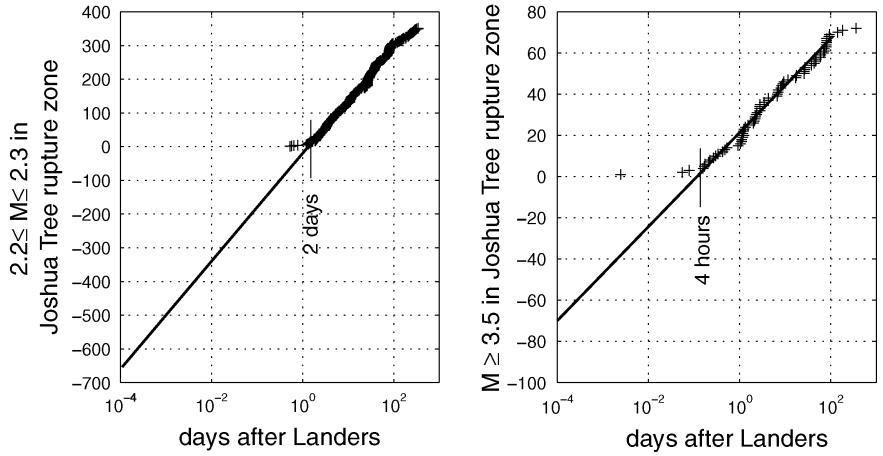

Figure 5
Occurrence times of the Landers aftershocks in the region under study (see Figure 4), vs. the index of the aftershock (i.e., cumulative number), for two magnitude intervals: (Left) $2.2 \leq M \leq 2.3$ and (right) $M \geq 3.5$. The thick lines are the best Omori fits (a $1/t$ decay of the aftershock rate, hence a $\log t$ increase of the cumulative number of aftershocks) for the 2 days–100 days (left) and 4 hours–100 hours (right) time intervals. These fits are extrapolated to short time scales to yield estimates of the number of aftershocks missed by the operator. At about 100 days, a clear decrease of the aftershock rate is observed in both magnitude bands.

region studied. The occurrence time t_i of the i^{th} aftershock follows a $\log t_i \sim i$ relationship related to the $1/t$ Omori decay of the aftershock rate, for t between (i) a 'detection' time (time at which the aftershocks can be discriminated amidst the strong seismic noise) that depends on the magnitude, and (ii) about 100 days. After 100 days, a clear decrease in activity is observed. This value is comparable to the six month interval of OGATA *et al.* (2003) who interpreted this reduced activity as resulting from shallow aseismic slip on the fault that was to seismically rupture during the 1999 Hector Mine earthquake.

An estimate of the number of aftershocks missed by the operator can be calculated by extrapolating the $\log t_i \sim i$ relation to short time scales. This assumes that Omori's law is valid down to short time scales. For a lower cut-off at 10^{-3} days $\simeq$ 1 mn 30 s, this indicates that about 500 earthquakes with magnitude between 2.2 and 2.3, and about 46 earthquakes with magnitude larger or equal to 3.5, have been missed in the first 2 days ($2.2 \leq M \leq 2.3$) or in the first 4 hours ($M \geq 3.5$), see Figure 5. These numbers are of the same order as the number of aftershocks effectively detected in the first 100 days of the sequence, cf. Figure 6. The fact that the relative number of missed aftershocks decreases with magnitude following an equivalent of a Gutenberg-Richter law, hence with no clear magnitude cut-off in the M 2.2+ range, can possibly explain the ubiquitous observation that the b value decreases immediately after the occurrence of a large earthquake.

Because so many aftershocks are likely to be missed in the first 2 days of the sequence, we cannot reliably study the triggering at this time scale. Unfortunately, the first hours/days are expected to be the time scales excited by dynamic triggering

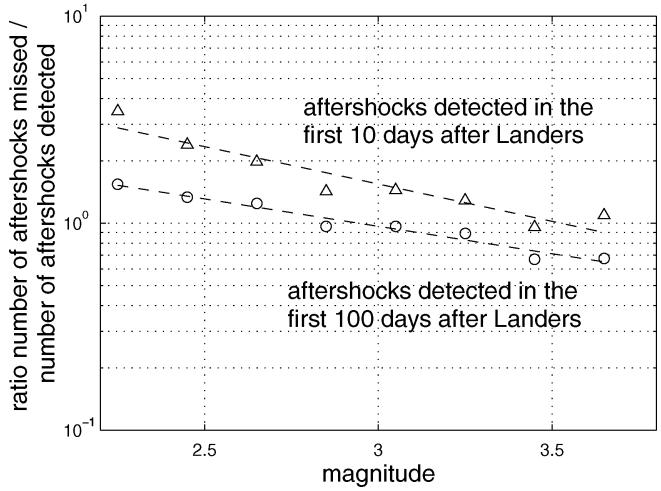

Figure 6
Ratio of the number of aftershocks missed to the number of aftershocks detected, for the first 10 days and 100 days following the Landers earthquake. The number of aftershocks missed is estimated by extrapolating Omori's law to 10^{-3} days $\simeq$ 1 mn 30 s after Landers, see Figure 5.

(BELLARDINELLI *et al.*, 2003). Three time intervals are thus analysed here: 2 days to 7 days (relatively short time scales that could still be influenced by dynamic triggering), 7 days to 100 days, and the complete 2 days to 100 days interval.

3.2 Rate Change Estimates

As discussed in section 2, rate change estimates are biased towards triggering, the more so when the number of earthquakes occurring prior to the main shock (here, the Landers earthquake) is low in the zone studied. A trade-off between very large zones (hence a weaker bias) and some spatial resolution has to be found. In this section we propose three ways of spatially discretizing the region: (1) a zonation in 13 zones, based on their level of seismicity, see Figure 7. These zones roughly correspond to clusters of events. This zonation is subjective, and is only intended to split the region in zones of similar orders of magnitude (tens to a few hundreds) in numbers of earthquakes. The small number of zones allows for a direct, visual inspection of the quality of the fit by the seismicity model (i.e., Omori-Utsu's law) for every zone. Note that some of the zones in Figure 7 (e.g., zone 8) have dimensions smaller or of the order of the estimated epicentral location error. This can lead to a bias in the rate change estimates for these zones. (2) A regular grid with 1 km

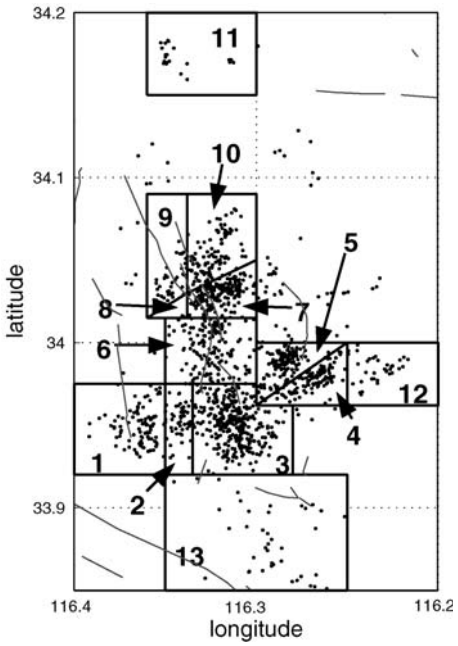

Figure 7
Zonation of the Joshua Tree region into 13 zones, plotted with the M 2.2+ earthquakes that occurred between the Joshua Tree and the Landers earthquake.

spacing; each grid node being the centre of a circular zone such that at least $N_{\min}$ M 2.2+ earthquakes are counted that occurred between the times of the Joshua Tree and the Landers earthquakes. To each node there thus corresponds a circular zone with a radius that changes from one node to the other. Two values for the $N_{\min}$ parameter are studied ($N_{\min} = 10$ and 40). (3) Finally, a search for seismicity shadows is specifically developed in section 3.5, that considers random sets of cells connected together on a regular grid.

In order to illustrate the method we first detail the analysis for zone 1.

Seismicity models: As described in section 2.1, a parameterised model of seismicity must first be fitted against the earthquake data, up to the time T_0 of the Landers earthquake (June 28, 1992). Given the very low level of seismicity in this region prior to the Joshua Tree earthquake (Fig. 4), the model is fitted starting on the April 22, 1992, date ($t = 0$). Figure 8, top graph, shows the M 2.2+ seismicity time series in the $[0, T_0]$ time interval for zone 1, along with the best power-law fit (i.e., Omori-Utsu relation) of the form $\lambda(t) = A \times (t + c)^{-p}$ yielding the $\lambda(0,t) = \frac{A}{1-p}\left[(t+c)^{1-p^*} - c^{1-p}\right]$ curve displayed (see equation (1)). The best parameter set $\{A^*, p^*, c\}$ maximises the Poissonian likelihood function L, as shown in the bottom graph of Figure 8. The likelihood function is defined as $\log L(A,p,c) = -\int_0^{T_0} dt\, \lambda(t) + \sum_{i=1}^{N} \log \lambda(t_i)$ where $T_0 = 66$ days and $\{t_i\}$ is the set of occurrence times of the $N = 92$ M2.2+ earthquakes in this zone for this time interval. Note that a 2-D grid search in the (p, c) plane is possible here, since A^* is bound to be equal to $N(1-p^*)/\left[(T_0 + c^*)^{1-p^*} - c^{*1-p^*}\right]$ (for $p^* \neq 1$). The confidence envelope is seen (Fig. 8, bottom graph) to be rather wide, a consequence of the limited ($N = 92$) number of earthquakes used in this inversion.

The ability of the best model $\{A^*, p^*, c^*\}$ to follow the dynamics of the aftershock time series is tested in a way partly similar to the residual analysis of OGATA (1988), cf. Figure 9: the set $\{t_i\}$ of earthquake occurrence times is transformed into a new set $\{\tau_i\}$ such that $\tau_i = \lambda(0, t_i) = \int_0^{t_i} dt\, \lambda(t)$, which should be a realisation of a stationary Poisson process if the tested model is perfect. Rather than displaying the distribution of the number of τ_i occurring in $[\tau, \tau + h]$ bins, with h arbitrarily fixed (OGATA, 1988), and testing its Poisson character, we here test whether the inter-event transformed 'times' $\Delta\tau_i = \tau_i - \tau_{i-1}$ (note that they are not 'times' as such, having the dimension of numbers) are independent realisations of a unit exponential distribution. A Kolmogorov-Smirnov (KS) test is conducted for this purpose, yielding a probability 0.06 that the set $\{\Delta\tau_i\}$ is effectively exponentially distributed (with mean equal to 1). The independence of the $\Delta\tau_i$ is tested by computing the linear correlation coefficient $\rho = \rho(\Delta\tau_i, \Delta\tau_{i+1})$ which maximizes the set of correlation coefficients $\rho(\Delta\tau_i, \Delta\tau_{i+n})$ with $n \geq 1$. Monte-Carlo simulations give a 0.61 probability that $\rho = 0.09$ can be obtained by chance, if the interevent times are effectively independent of each other.

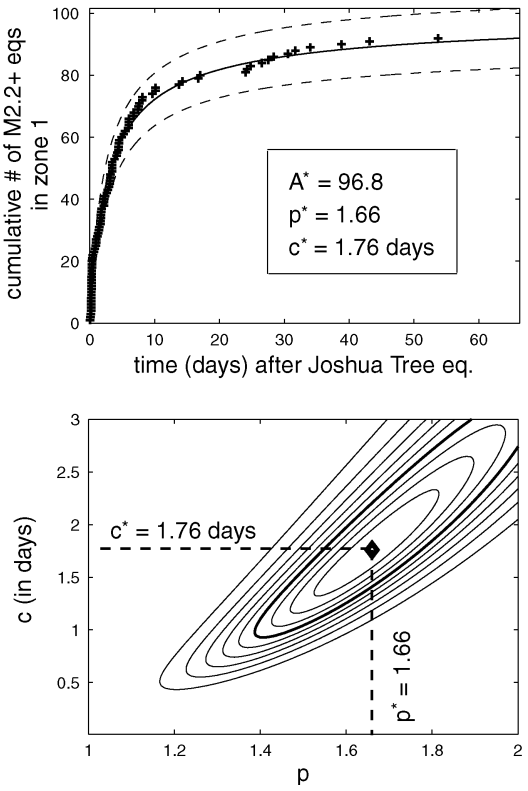

Figure 8
(Top) Best power-law (Omori-Utsu) fit of the M 2.2+ aftershocks (+) of the Joshua Tree earthquake in zone 1 (Fig. 7), computed for the 66 day-long time interval between the Joshua Tree and the Landers earthquakes (shown in cumulative numbers). Dashed line: One standard deviation away from the mean for a Poisson law with mean given by the best power-law fit. (Bottom) Iso-likelihood contours, in 0.1 steps, in the (p, c) plane, for the seismicity data of top graph. The best fit is indicated with a diamond, and is given a likelihood of 1. The confidence interval (60.6% likelihood) is shown in thick line.

While the fit shown in Figure 8 looks satisfactory, the tests show that the transformed times $\{\tau_i\}$ are not too well described by a Poisson process. Inspection of Figure 9 clearly shows that the early part of the sequence is characterised by a sudden and short acceleration (from the 4$^{\text{th}}$ to the 20$^{\text{th}}$ events) not well accounted for by the model. Such a feature, probably corresponding to the activation of a secondary aftershock cluster, is responsible for the low score at the Kolmogorov-Smirnov test. The part of the sequence starting from the 21$^{\text{st}}$ earthquake is however well approximated by the model: the same tests yield $P(KS > 0.107) = 0.36$ and $P(|\rho| > 0.017) = 0.93$ on this subset. Given that the model is intended to predict the seismicity at $t \geq T_0$, it can therefore be considered as a reliable model.

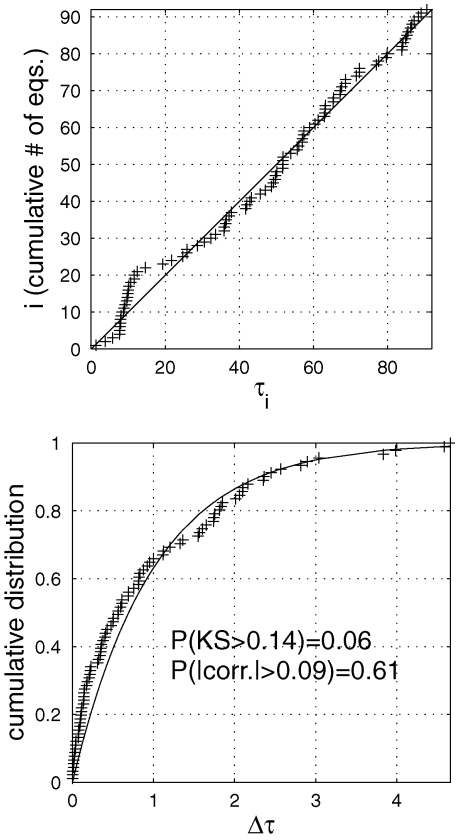

Figure 9
(Top) Earthquake index i vs. transformed time τ_i, for the best model of Figure 8. In the null hypothesis of a perfect model, the τ_i should randomly fluctuate near the $y = x$ line. (Bottom) Cumulative distribution of the increments $\Delta\tau_i = \tau_i - \tau_{i-1}$ (+), along with the exponential distribution (unit mean and variance) expected for a perfect model (continuous line). The Kolmogorov-Smirnov test indicates a probability of 0.06 that the maximum departure (0.14) from the exponential distribution is due to pure luck. The correlation coefficient $\rho = \rho(\Delta\tau_i, \Delta\tau_{i+1})$ is 0.09, and can be obtained with a probability of 0.61 by pure luck if the $\Delta\tau_i$ were mutually independent.

The ETAS model $\lambda(t) = \mu + A\frac{p-1}{c^{1-p}} \sum_{0 \le t_i \le t} e^{\alpha(m_i - m_c)}(t + c - t_i)^{-p}$ where $m_c = 2.2$ is the completeness magnitude, and $\{\mu, A, \alpha, c, p\}$ is the parameter set, is also fitted against the same data (Fig. 10). This model does better than the best Omori-Utsu model of Figures 8 and 9. The best ETAS parameters however give an unstable model, since the branching ratio $\frac{A^*\beta}{\beta - \alpha^*}$, where $\beta = b\log_{10}$ with the b value equal here to 1.25 for this zone, is higher than 1. This branching ratio is the mean number of earthquakes directly triggered by a trigger earthquake with magnitude following the Gutenberg-Richter distribution. For branching ratios > 1, the development of the

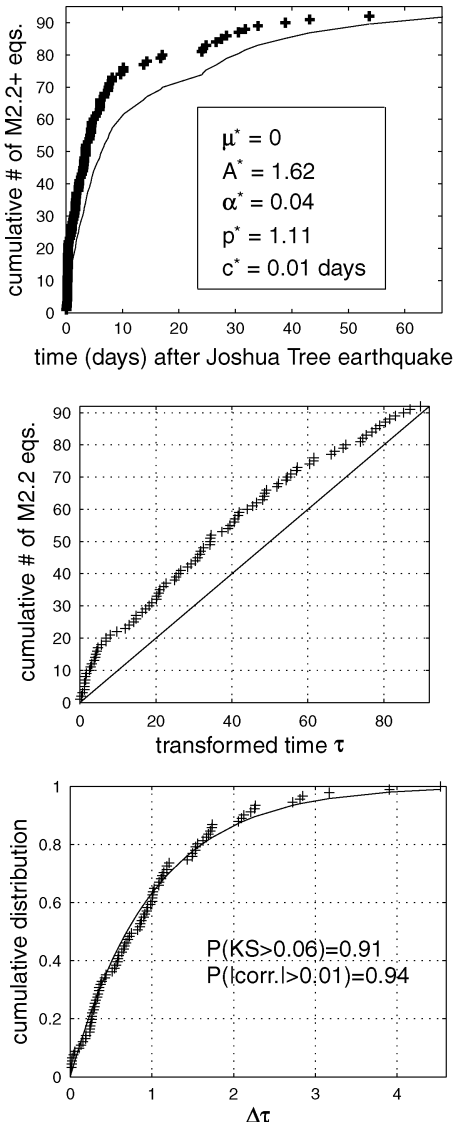

Figure 10
Same as Figures 8 and 9, for the ETAS model.

cascade of triggered earthquakes (1st generation, 2nd generation, and so on) blows up, and the mean total number of triggered events becomes infinite. Given the need in the present work to forward model the seismicity time series (see below), such an unstable model has to be discarded. The best parameter set such that $\frac{A^*\beta}{\beta-\alpha^*} \leq 1$ is therefore searched for, yielding $A^* = 0.96$, $\alpha^* = 0.09$, $p^* = 1.26$, $c^* = 0.01$ days, and

$\mu^* = 0.172$ per day. The tests then yield that $P(KS > 0.096) = 0.38$ and $P(|\rho| > 0.034) = 0.824$.

The rather unusually low values of α^* obtained for the two best ETAS models of above show that to assume the onsets of the secondary aftershock sequences to systematically coincide with the earthquake occurrence times $\{t_i\}$ is not pertinent: such a low value of α^* corresponds to a lack of correlation between the strength of the secondary aftershock sequence (i.e., number of aftershocks triggered) and the trigger magnitude, hence no direct causality between the two. Also, the Joshua Tree earthquake that primarily triggered this seismicity is not located in this zone, hence it is not included in the set $\{t_i\}$; the first ten earthquakes in zone 1 have magnitudes ranging between 2.2 (m_c) and 2.6. The model struggles to explain the onset of the sequence since there are no obvious triggers located in zone 1.

A solution to this problem without resorting to even less robust, more complex space-time models, is to propose a hybrid model with an Omori-Utsu rate function starting at $t = 0$, representing the action of the Joshua Tree earthquake, along with an ETAS model that reproduces local secondary, tertiary, ..., aftershock sequences. The model then writes $\lambda(t) = \mu + A\frac{p-1}{c^{1-p}} \sum_{0 \le t_i \le t} e^{\alpha(m_i - m_c)}(t + c - t_i)^{-p} + A_0(t + c_0)^{-p_0}$. For consistency and simplicity, we assume that $p_0 = p$ and $c_0 = c$, and take $\mu = 0$ since very little seismicity existed in the region before the Joshua Tree earthquake. The five remaining parameters $\{A_0, A, \alpha, p, c\}$ are then inverted for. This inversion indicates that the Omori-Utsu contribution $A_0(t + c)^{-p}$ is dominant, with $A_0^* \simeq 114$, while $A^* \simeq 0.02$. The much higher value of $\alpha^* = 2.9$ as compared to previously indicates that the model can now find causal triggering in the local secondary aftershock sequences of this zone. However, this best hybrid model behaves very similarly to the best Omori-Utsu model, and therefore will not be further considered in this study.

Expected (predicted) seismicity rates and shadow detectability: We now use the Omori-Utsu model to predict the mean λ_0 that would be expected in $[T_0 + \delta_1, T_0 + \delta_2]$, by extrapolating the model to this time interval. As mentioned, three time windows are considered: (i) from $\delta_1 = 2$ days to $\delta_2 = 7$ days, (ii) from $\delta_1 = 2$ days to $\delta_2 = 100$ days, (iii) from $\delta_1 = 7$ days to $\delta_2 = 100$ days. To estimate the pdf $f_0\left(\hat{\lambda}_0\right)$ of the estimated $\hat{\lambda}_0$, we explore the parameter space (p, c) within and around the envelope error (Fig. 8), compute $\hat{\lambda}_0(\theta) = \int_{T_0+\delta_1}^{T_0+\delta_2} dt\, \lambda(t)$ for each parameter set θ, and construct $f\left(\hat{\lambda}_0\right)$ as

$$f\left(\hat{\lambda}_0\right) \int d\theta\, L(\theta) = \int d\theta\, L(\theta)\, \delta\left(\hat{\lambda}_0 - \hat{\lambda}_0(\theta)\right), \tag{13}$$

where $L(\theta)$ is the likelihood of θ given the data, and $\delta(.)$ is the generalised Dirac function. The pdf are shown in Figure 11, along with an estimate of the minimum detectable shadow, for a significance level of $\gamma_m = -2$ (see section 4). No shadow is

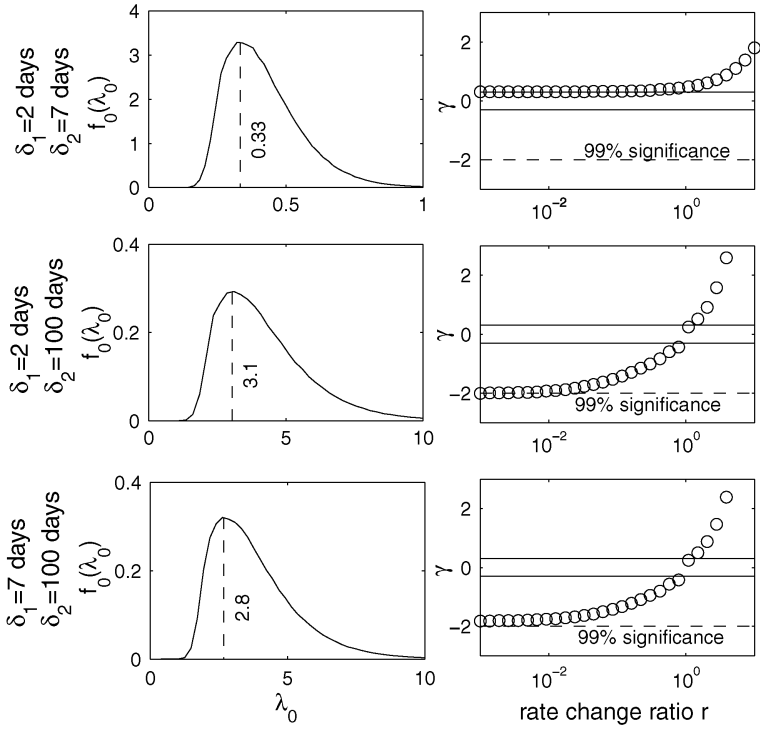

Figure 11
Probability density function $f_0(\hat{\lambda}_0)$ (left) and significance level γ vs. rate change ratio r (right) for the three time intervals $[T_0+\delta_1, T_0+\delta_2]$ studied, for zone 1. The detectability of seismicity shadow with a minimum significance level of 99% ($\gamma \leq -2$) is indicated. Only in the 2 days–100 days interval are shadows potentially detectable with a 99% significance.

detectable in the first week (at the 99% significance level), while rate decreases with ratio less than about 0.01 are detectable with significance $\gamma \leq \gamma_m = -2$ (hence a 99% significance level or better) when $\delta_1 = 2$ days and $\delta_2 = 100$ days. These shadows, if they exist, will be seen with a bias on $E\{\log_{10} \hat{r}\}$ of at least $+1.62$.

Observed seismicity rates: The numbers m of earthquakes actually observed in the three $[T_0+\delta_1, T_0+\delta_2]$ intervals are 12, 44, and 32, respectively, for zone 1. Given those numbers, the pdf of the actual Poisson mean estimate $\hat{\lambda}_1$ is constructed using equation (4). These pdf $f_1\left(\hat{\lambda}_1\right)$ are centered on much larger values of $\hat{\lambda}$ than $f_0\left(\hat{\lambda}_0\right)$: the observed numbers m are not well explained by the *a priori* rates λ_0. This zone has very clearly undergone a strong increase of seismicity following the Landers earthquake, for the time intervals studied.

Seismicity rate change estimates and significance: Given the two pdf $f_0\left(\hat{\lambda}_0\right)$ and $f_1\left(\hat{\lambda}_1\right)$ estimated for each time interval, we now estimate the β, Z, $\mathscr{P}$ and γ statistics described in section 2.3. These statistics measure the significance of the rate change.

Various ways of computing the β statistic can be proposed. In the original form by MATTHEWS and REASENBERG (1988), cf. equation (2), we obtain $\beta = (m - \lambda_0^*)/\sqrt{\lambda_0^*}$ with λ_0^* the maximum likelihood estimate of λ_0 (i.e., yielding the maximum of $f_0\left(\hat{\lambda}_0\right)$, cf., Figure 11). For example, in the [2 days, 7 days] interval, $\lambda_0^* \simeq 0.33$, which yields $\beta = 18.8$. A first sophistication is given by considering the full pdf of $f_0\left(\hat{\lambda}_0\right)$ rather than just λ_0^*, see equation (3). We here go a step further by computing β as $\beta = \int_0^\infty d\hat{\lambda}_0 f_0\left(\hat{\lambda}_0\right) \int_0^\infty d\hat{\lambda}_1 f_1\left(\hat{\lambda}_1\right) \frac{\hat{\lambda}_1 - \hat{\lambda}_0}{\sqrt{\hat{\lambda}_0}}$. In the case of the [2 days, 7 days] interval, we then obtain $\beta = 20.1$. A very similar calculation is done for the statistic Z, which, by extension of equation (10), is given by $Z = \int_0^\infty d\hat{\lambda}_0 f_0\left(\hat{\lambda}_0\right) \int_0^\infty d\hat{\lambda}_1 f_1\left(\hat{\lambda}_1\right) \frac{\hat{\lambda}_1 - \hat{\lambda}_0}{\sqrt{\hat{\lambda}_0 + \hat{\lambda}_1}}$. This gives $Z = 3.38$ for this time interval. Finally, the probability of triggering given by equations (6) and (7) is estimated to be in the interval $1 - 10^{-14} \leq \mathscr{P} \leq 1$, hence $\gamma \geq 14$, see equation (8); this value of γ is here bounded by the floating type precision of 10^{-14} used in this computation. Overall, all these statistics agree with a strongly significant seismicity increase.

The rate change itself is estimated using equation (9), to $E\{\log_{10} \hat{r}\} = 1.50$, still for the [2 days, 7 days] interval following Landers. Note that the maximum likelihood estimate m/λ_0^* is equal to $10^{1.56}$. Table 1 summarizes these results for the three observation intervals, for zone 1. Triggering is found to characterize this zone, at the time scales examined.

3.3 Mapping Seismicity Changes

The analysis is now extended to the remaining 12 zones, using the Omori-Utsu model, and (for zone 11) a double Omori-Utsu law (one starting at the time of the Joshua Tree earthquake, plus a second one starting 48 days later, when a local cluster containing a M 4.4 earthquake initiated). Figure 12 summarizes the results of this analysis. We see that triggering is mostly observed, being very significant at all three time intervals for 6 zones (1, 3, 6, 8, 9, 13). Five zones (2, 4, 7, 11, 12) experience

Table 1

Results of the analysis for zone 1, for three time intervals $[T_0 + \delta_1, T_0 + \delta_2]$ (1st column); m is the number of observed earthquakes in the interval. The detectability of seismicity shadows is assessed for a minimum 99% *significance level ($\gamma \leq \gamma_m = -2$); the maximum ratio r detectable is indicated (along with the minimum bias on the $E\{log_{10}\hat{r}\}$ estimate). The rate change estimates are $E\{log_{10}\hat{r}\}$ and the maximum likelihood estimate $log_{10}r$ (in parenthesis). A value of 14 for γ indicates that $\gamma \geq 14$: 10^{-14} is the maximum precision on the floating type for the mathematical software used in this analysis*

Time interval	m	Detectability	Rate change estimates	β	Z	γ
2 days–7 days	12	no detectable shadow	1.50 (1.55)	20.1	3.38	14
2 days–100 days	44	r<0.01 (bias $\geq$ 1.62)	0.06 (1.20)	21.1	5.79	14
7 days–100 days	32	no detectable shadow	0.97 (1.11)	16.0	4.79	14

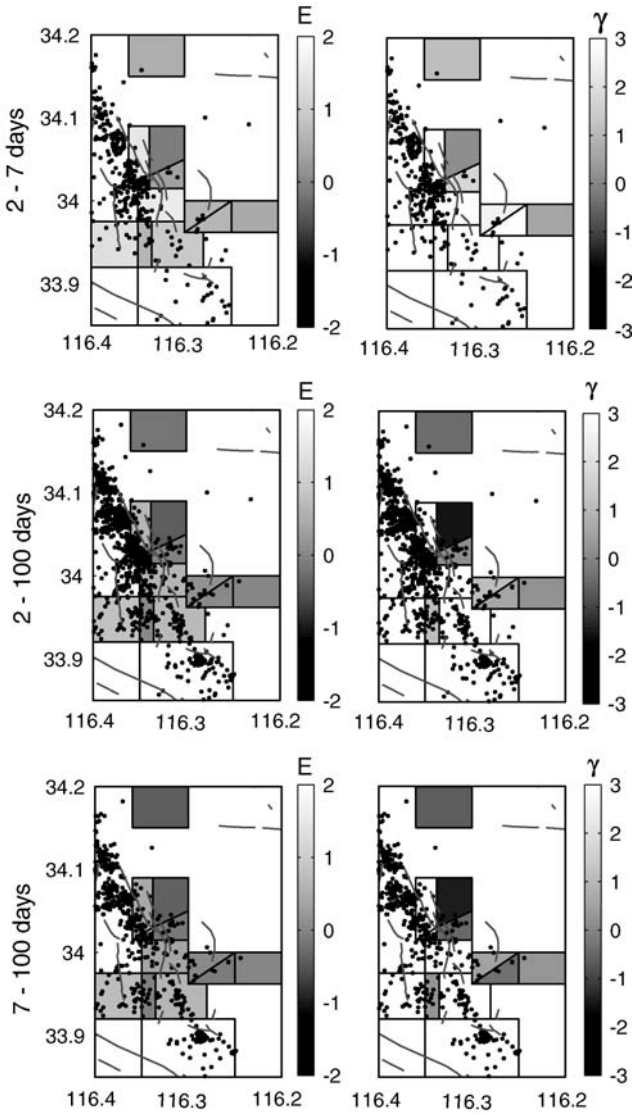

Figure 12
(Left) Mean logarithm of the rate change ratio $E\{\log_{10}\hat{r}\}$, with (right) γ as a measure of the significance of the change, for the three time intervals 2–7 days, 2–100 days, 7–100 days, for the 13 zones.

significant triggering in the 2 days–7 days interval, followed by a decrease in the 7 days–100 days interval. The latter is however not significant, with the exception of zone 11.

The only cases of significant seismicity decrease are obtained for 2 zones (zones 10 and 11) for the 2 days–100 days and the 7 days–100 days intervals. Since no

shadow is detectable at the 99% significance level in the first week for all 13 zones, it cannot be known whether these zones also underwent a shadow at this time scale.

However, the best seismicity model used for zone 10 does not provide a good fit to the data. A clear slow-down of the aftershock activity following the Joshua Tree earthquake occurred in this zone about 30 days prior to the Landers earthquake, cf. Figure 13. It is, therefore, a possibility that the observed shadow is not related to the occurrence of the Landers earthquake. Zone 11 is a clearer case of a possible shadow, since a complete shutdown of the activity is observed after 2 days in this zone.

In order to study the influence of the spatial discretisation of the seismicity, the rate changes are also estimated for a regular grid with 1 km spacing between nodes. For each grid node, a circular region is selected such that at least $N_{\min}$ M 2.2+ earthquakes occurred in it, between the Joshua Tree and the Landers earthquakes. Then the best Omori-Utsu fit is found for this circular zone, and the grid node is

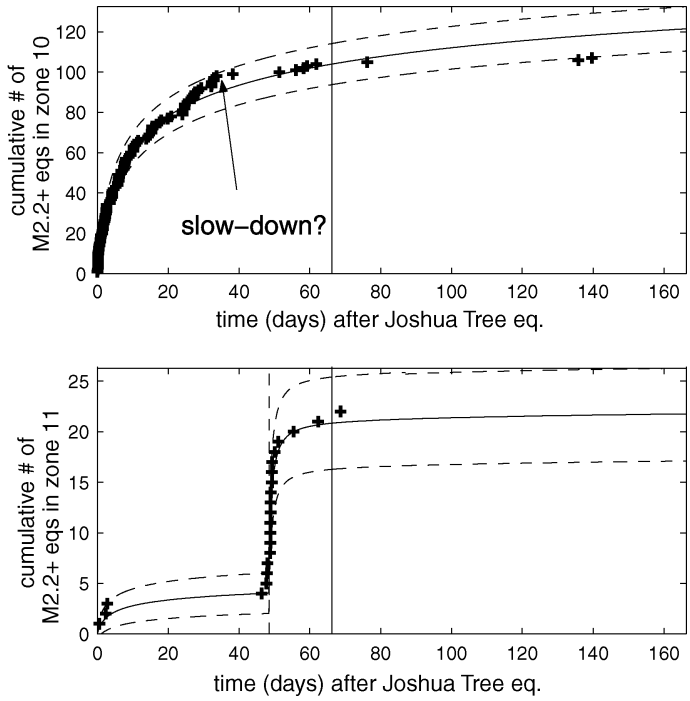

Figure 13
Best power-law (Omori-Utsu) fit of the M 2.2+ aftershocks (+) of the Joshua Tree earthquake in zones 10 and 11, fitted against the 66 day-long time interval between the Joshua Tree and the Landers earthquakes (shown in cumulative numbers) and extrapolated up to 100 days after the Landers earthquake. Dashed line: One standard deviation from the mean for a Poisson law with mean given by the best power-law fit. The occurrence time of the Landers earthquake is shown by the vertical line at about 66 days. An apparent slow-down of the activity about 30 days prior to the Landers earthquake is observed for zone 10.

given the resulting $E\{\log_{10}\hat{r}\}$ and γ values. Figure 14 shows the results of this analysis, for $N_{\min} = 10$, for the 2 days–100 days time interval. The rate change estimates are roughly the same as with $N_{\min} = 40$ (not shown here) and with Figure 12, apart from the very north of the region (corresponding to zone 11). In that case $N_{\min} = 40$, and since little seismicity occurred there between the two main shocks, the radius of the circle is relatively large (of the order of 7 km). Part of the main Landers aftershock zone is then probed, resulting in considerably higher seismicity rate changes than with $N_{\min} = 10$. This example shows the uncertainty and lack of resolution of this method in regions with little seismicity.

The clearest instances of seismicity quiescences roughly correspond to zones 4, 10 and 11 of Figure 7. However, as already mentioned, the quiescence of zone 10 appears to start about 30 days prior to the occurrence of the Landers earthquake. To investigate this point, we performed the same analysis as in Figure 14, but for the 30 days before Landers (29/5/1992–27/6/1992). The best Omori-Utsu fits are found for the time interval following the Joshua Tree earthquake and before

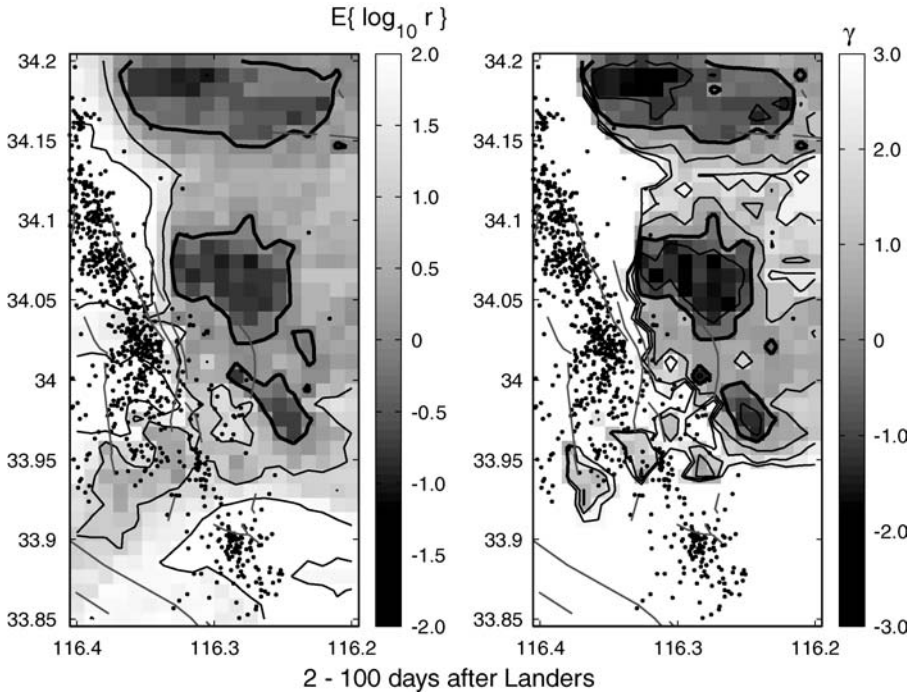

Figure 14
Seismicity rate changes for the time interval 2 days–100 days after the occurrence of the Landers earthquake, using $N_{\min} = 10$: (Left) $E\{\log_{10}\hat{r}\}$ and (right) γ. Iso-contours are shown with a unit step, the zero contour being drawn with a thick line. Superimposed is the M 2.2+ seismicity that occurred during this time interval. The three zones with clear ($\gamma < -1$) quiescence roughly correspond to zones 4, 10 and 11 (from south to north) of Figure 7.

29/5/1992, and are then extrapolated to the following one month. Figure 15 shows that clear quiescence is found in zones 2, 4 and 10 (cf., Fig. 7). They therefore do not coincide with the occurrence of the Landers earthquake. This confirms that most of the quiescence shown in Figure 14 is not caused by Landers, but precedes it. On the contrary, the northernmost zone (corresponding to zone 11) experienced strong triggering in the 29/5/1992 – 27/6/1992 interval, related to the occurrence of a local cluster of earthquakes, before being put in a quiet mode by the Landers earthquake.

3.4 Comparison with Coulomb Stress Changes

The changes in static stress due to the occurrence of the Landers earthquake are shown in Figure 16, for the two slip distributions detailed in WALD and HEATON (1994) and HERNANDEZ *et al.* (1999). In order to compare two different approaches for selecting a target fault plane, we computed the Coulomb stress changes for optimal, vertical, dextral strike-slip faults (hence only the strike angle is left free to

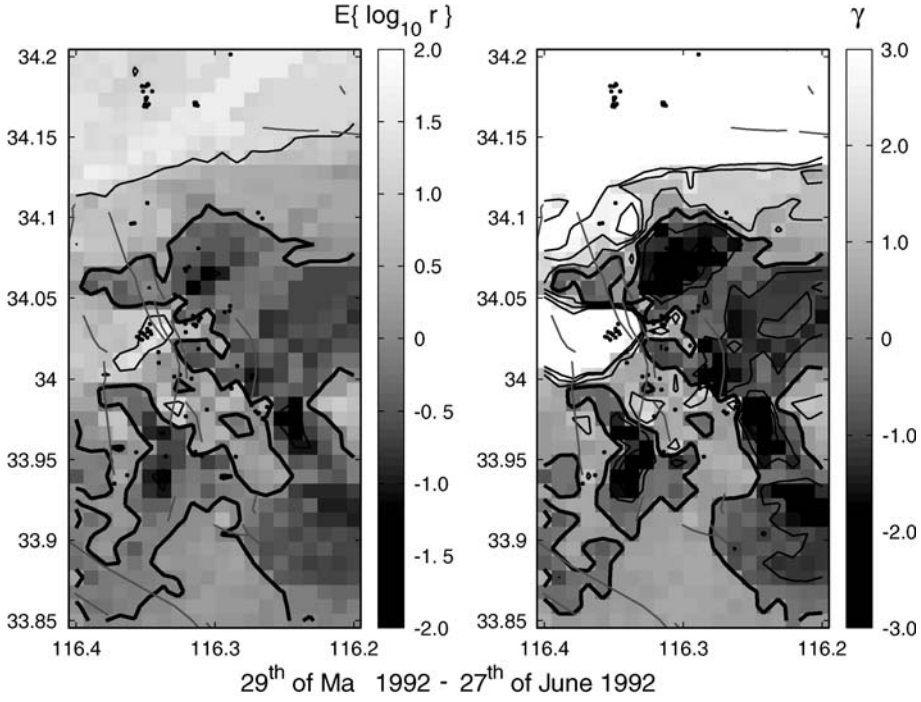

Figure 15
Same as Figure 14, but for the 1-month interval prior to the occurrence of the Landers earthquake. The M 2.2+ seismicity that occurred in this time interval is plotted. Two clear instances of quiescence (corresponding to zones 4 and 10 of Figure 7), that thus started one month before the Landers earthquake, are observed here and also on Figure 14.

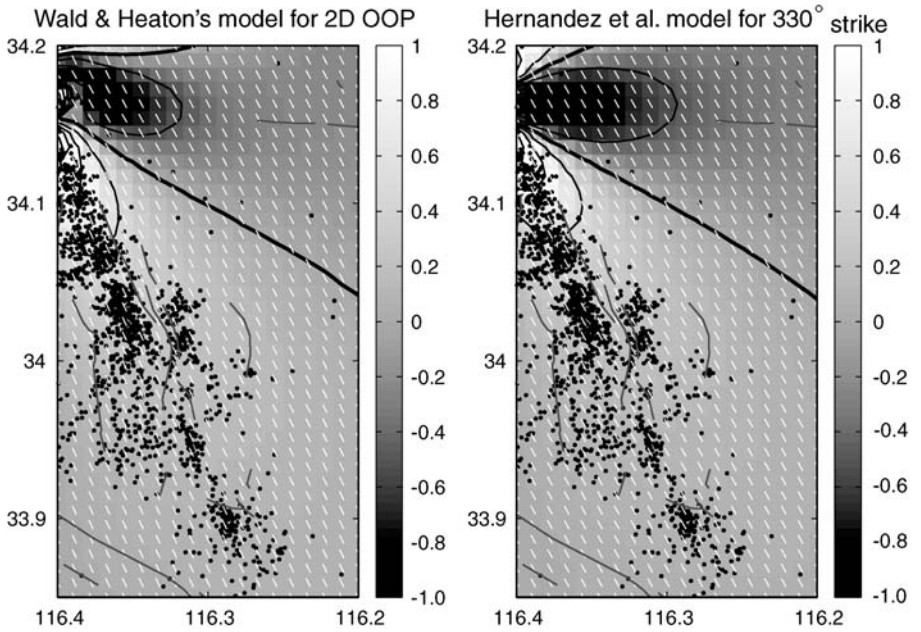

Figure 16
Coulomb stress changes in MPa due to the Landers earthquake, computed at 7.5 km depth, for a friction coefficient $\mu = 0.4$. (Left) Slip distribution from WALD and HEATON (1994), with stress projected on optimally-oriented vertical, dextral strike-slip faults. (Right) Slip distribution from HERNANDEZ *et al.* (1999), with stress projected on vertical, dextral strike-slip faults striking at 330° north. Iso-contours are shown at every 0.5 MPa interval. The 0 MPa contour is shown with a thick line. The strikes of the target faults are shown with the white segments. The M 2.2+ earthquakes that occurred in the first 100 days following the Landers earthquake are plotted.

vary) and for imposed vertical, dextral strike-slip planes striking at 330° north (corresponding to the mean strike angle in this zone following the Landers earthquake, see HAUKSSON, 1994 and Fig. 17). In the first case, a regional compressive stress of 100 bars oriented at N7°E is assumed, following STEIN *et al.* (1992) and HARDEBECK and HAUKSSON (2001). The effective coefficient of friction is set to $\mu = 0.4$. Only minor changes are seen between the two stress maps, indicating that these stress calculations are reasonably robust. A good correlation is seen with the northernmost quiescence zone of Figure 14. We recall here that only this quiescence zone seems to be related to the Landers earthquake, while the diminished activation of the more central zone as observed in Figures 14 and 15 started about 1 month prior to the Landers earthquake. In Figure 18 we compare the changes in Coulomb stress with the changes in seismicity rates. A clear correlation is found this correlation increases if the central quiescent zones are discarded from the plot, as their seismicity decreased one month prior to rather than at the time of occurrence of the Landers earthquake.

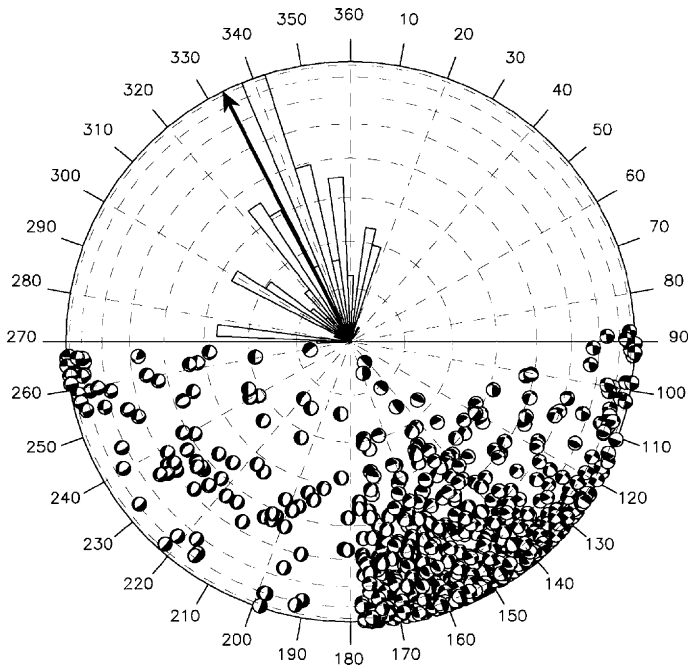

Figure 17
Rose diagram showing (upper semicircle) the distribution of orientations of structures (California Department of Conservation, 2000) which experienced recent (Quaternary, Holocene or historical) seismicity, and (lower semicircle) the distribution of the focal mechanisms of the M 2.2+ earthquakes that occurred in the 2 days–100 days time interval after the Landers earthquake (data from HAUKSSON, 2000). A 180° angle is added or substracted to the strike angle if necessary, to keep it in its semicircle. The radial bars in the upper semicircle are proportional to the number of 1-km structural elements in each particular orientation. The arrow in the upper semicircle indicates the mean strike of the aftershocks.

3.5 Detection of Seismicity Shadows

A specific procedure is now described, that search for seismicity shadows. As explained in section 2.4, such a search must be conducted over (connected) regions with any possible shape, i.e., not necessarily circular or square. It is clear that a direct consequence of optimizing the zones for finding seismicity shadows is that it creates a bias towards quiescence. This is intentionally done in order to compensate for the natural bias towards triggering that is discussed in Section 2.4. We first discretise the region into 2 km cells; the grid spacing being of the same order as the earthquake location error estimate. Then, starting with any one cell, we perform a random walk over the grid. This walk randomly draws clusters, counting N cells. For each of these clusters, we apply the method detailed in 3.2: (i) the best Omori-Utsu law is searched for, that best mimics the earthquake time series of the cluster between the time of the Joshua Tree earthquake to the time of the Landers earthquake, (ii) the two pdf

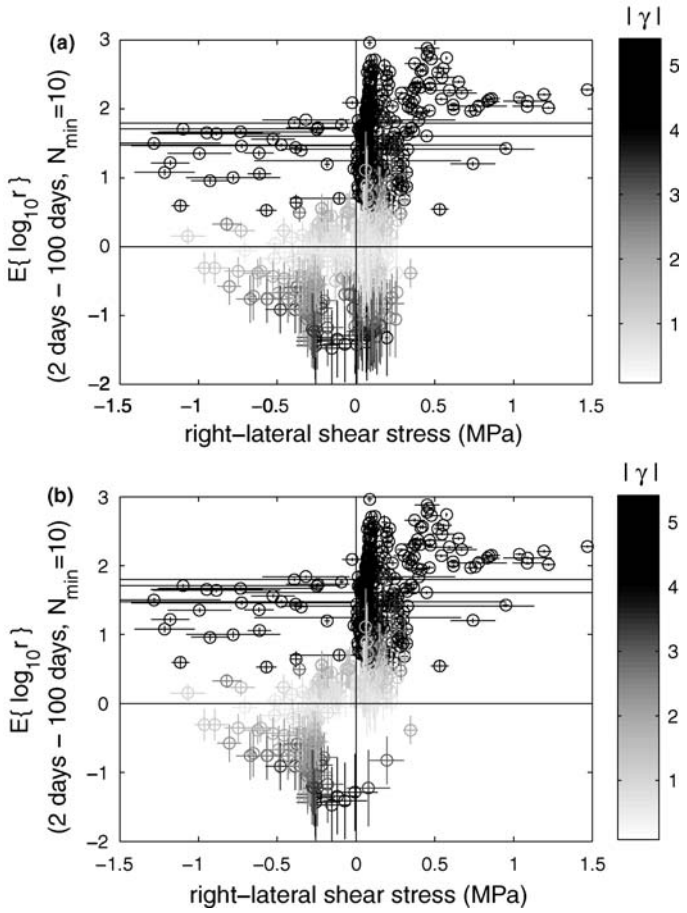

Figure 18

$E\{\log_{10}\hat{r}\}$ for the 2 days–100 days interval following Landers, vs. the Coulomb stress change due to the Landers earthquake, in MPa. Both types of changes are computed over a regular grid with 1 km spacing. We used $N_{\min} = 10$ for the seismicity rate changes (cf. Fig. 14). The dots are colored according to the significance γ of the seismicity change. Error bars are displayed, that correspond vertically to the standard deviation of $\log_{10}\hat{r}$, and horizontally to half the difference between the stress values of the two graphs shown in Figure 16, computed for two different slip distributions and for two types of target fault plane geometries. (Top) Plot for all the 19×39 cells, (Bottom) plot after discarding the cells showing quiescence in the central zone that are related to a deactivation that took place about 1 month before the Landers earthquake.

$f_0\left(\hat{\lambda}_0\right)$ and $f_1\left(\hat{\lambda}_1\right)$ are estimated, and (iii) $E\{\log_{10}\hat{r}\}$ and γ are computed. This procedure is conducted for $N \leq 20$, and 100 random walks are performed for each initial cell. Then, the minimum $E\{\log_{10}\hat{r}\}$ (with a significance of at least 99%) and the corresponding γ are kept, that is, each cell 'keeps' the lowest, 99% significant, $E\{\log_{10}\hat{r}\}$ value of all the clusters it belongs to. If no seismicity decrease with a 99% significance is found for a cell, then the lowest $E\{\log_{10}\hat{r}\}$ is kept.

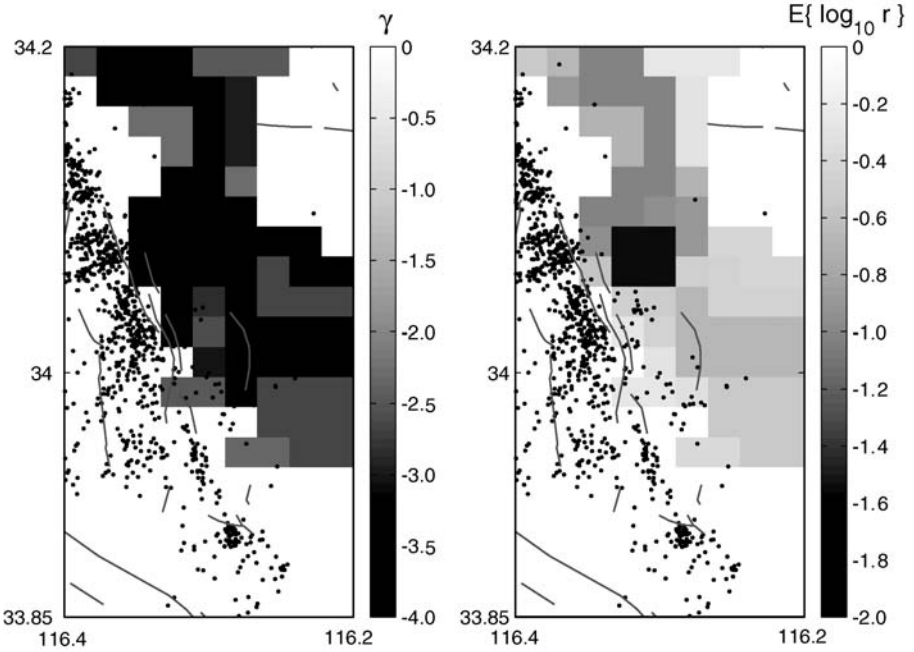

Figure 19
Minimim significance measure γ and $E\{\log_{10}\hat{r}\}$ obtained for the 7 days–100 days time interval after the Landers earthquake, using the method described in 3.5. The dots are M 2.2+ earthquakes occurring in this time interval.

This procedure is run for the 7 days – 100 days interval, as being the time interval (of the three examined in 3.2) most likely to be characterised by seismicity shadows. Figure 19 presents the results of this analysis. Seismicity shadows with a significance above the 99% level ($\gamma < -2$) are clearly seen, extending —at least partly— over zones 4, 5, 7, 9, 10, 11 and 12. The corresponding seismicity rate log-ratio $E\{\log_{10}\hat{r}\}$ are estimated to values typically ranging from -0.5 to -1.5. It is important here to recall that these estimates are model dependent, other values would be obtained if using other seismicity models. It must be noted that this method, which optimizes the zones for detecting quiescence, does not substantially change the results obtained with the 'non-optimized', and more classical method of Section 3.3, at least for the present case study.

4. Conclusions

The general methodology for estimating seismicity rate changes is now well developed. A variety of statistical measures have been proposed that test the significance of the changes and indicate whether rate decreases are potentially

detectable or not. This methodology was applied in section 3 to a particularly interesting situation, where a large magnitude earthquake (the M_w 7.3 Landers earthquake) occurs not long after a first strong shock (the M_w 6.1 Joshua Tree earthquake) had already triggered an important earthquake activity. There are several advantages when analysing this type of situation. Seismicity shadows are more easily detectable. Also, the earthquake time series can be modeled, to a correct approximation, by a simple Omori-Utsu law, starting at the time of the first shock. Finally, an analysis at small scales (down to the earthquake location error scale) and short times (days) can be performed, thus yielding a rather detailed picture of the changes brought by the Landers earthquake in this area.

Interestingly, we observed seismicity shadows developing after a few days (one week), sometimes preceded by instances of early triggering. This could be, as proposed by MARONE (2000), a way of proving the existence of dynamically triggered aftershocks. An analysis of other historical doublets (the 1999 Izmit and Ducze earthquakes) and multiplets (the 1997 Colfiorito sequence) will be developed elsewhere.

The most evident limitation to seismicity change analyses is that they are model-dependent. The null hypothesis of 'no change' is constructed by extrapolating the earthquake time series to the time interval studied. This extrapolation requires the use of a model that 'best' mimics the observed time series up to the time of what is considered as the trigger (e.g., main shock). There is at present a very strong need for the development of space-time models (e.g., ZHUANG *et al.*, 2002) that can be inverted quickly and robustly, and that can be forward simulated at low computational costs. It can be hoped that the use of such an efficient model, together with better quality data (e.g., earthquake data with more accurate location estimates, for example using recent relative location methods), could lead to considerably more detailed analyses, and to a far better understanding of how faults interact.

Acknowledgements

We would like to thank Karen FELZER for reviewing an early version of this manuscript, Christophe VOISIN, Fabrice COTTON, and Jochen WOESSNER for providing preprints of their works, and Andy MICHAEL, an anonymous reviewer and Yehuda BEN-ZION for helpful comments and suggestions. Use of the SCSN seismicity catalogue (hosted by the SCEC web site) is acknowledged.

Appendix

Detectability of Seismicity Shadows

We assume in this section that the seismicity model is perfect, so that the distribution of the estimate $\hat{\lambda}_0$ of λ_0 is concentrated on λ_0: $f_0\left(\hat{\lambda}_0\right) = \delta\left(\hat{\lambda}_0 - \lambda_0\right)$. The

detectability of a seismicity change function of the duration $\Delta = \delta_2 - \delta_1$ of observation can be investigated by computing the ensemble average of γ (measure of the significance) and the mean log-ratio change $E\{\log \hat{r}\}$. This can be synthetized as follows:

- The expected number of earthquakes in the time interval Δ given by the null hypothesis is a Poisson random variable with mean $\Lambda_0 = \lambda_0 \Delta$. In the following development, the notation λ will refer to the mean number per unit time, and $\Lambda = \lambda \Delta$ to the mean number for the duration Δ.
- The ratio r of the seismicity change is fixed, so that the observed number m of earthquakes in Δ is a realisation of the Poisson distribution with mean $\Lambda_1 = r\Lambda_0$.
- Given one observation of this process, hence given one realisation of m, the estimate $\hat{r}$ such that $\hat{\Lambda}_1 = \hat{r}\Lambda_0$ is the estimated rate in Δ, has the pdf $f(\hat{r}|m) = \Lambda_0 \exp(-\hat{r}\Lambda_0)(\hat{r}\Lambda_0)^m/m!$.
- From this distribution, the observer can deduce $E\{\log \hat{r}\}$ and γ using equations (8) and (9).
- On ensemble average, an infinitely large set of realisations of this process leads to an infinite number of observers seeing various numbers m of earthquakes occurring in Δ, with probability $P(m) = \exp(-r\Lambda_0)(r\Lambda_0)^m/m!$. This gives the following

$$E\{\log \hat{r}\} = -\log \Lambda_0 + \sum_{m=0}^{\infty} e^{-r\Lambda_0} \frac{(r\Lambda_0)^m}{m!} \int_0^{\infty} dx \, \frac{x^m}{m!} e^{-x} \log x \tag{14}$$

and

$$\mathscr{P} = 1 - \sum_{m=0}^{\infty} e^{-r\Lambda_0} \frac{(r\Lambda_0)^m}{m!} P(m+1, \Lambda_0) \tag{15}$$

on ensemble average, with $P(.,.)$ being the incomplete Gamma function.

The dependence of these measures on the duration Δ can then be studied by numerically estimating these two quantities. Figure 2 was computed for $\lambda_0 = 2$ earthquakes per year, and by letting the duration of observation Δ varying from 0 to 10 years. Three values of r were considered: $r = 100$ (triggering), $r = 1$ (no changes) and $r = 0.01$ (inhibition). In the case of Figure 3, Δ was held constant at 2.4 years, and r was allowed to vary.

References

Belardinelli, M.E., Bizarri, A., and Cocco, M. (2003), *Earthquake Triggering by Static and Dynamic Stress Changes*, J. Geophys. Res. *108*, 2135.

California Department of Conservation, *Digital database of faults from the fault activity map of California and adjacent areas*, Div. of Mines and Geol (Publication CD 2000–006, Sacramento, 2000).

DIETERICH, J., CAYOL, V., and OKUBO, P. (2000), *The Use of Earthquake Rate Changes as a Stress Meter at Kilauea Volcano*, Nature *408*, 457–460.

FELZER, K.R., ABERCROMBIE, R.E., and BRODSKY, E.E. (2003), *Testing the stress shadow hypothesis*, EOS Trans. AGU *84(46)*, Fall Meet. Suppl., Abstract S31A-04.

GOMBERG, J., REASENBERG, P.A., BODIN, P., and HARRIS, R.A. (2001), *Earthquake Triggering by Seismic Waves Following the Landers and Hector Mine Earthquakes*, Nature *411*, 462–466.

HABERMANN, R.E. (1983), *Teleseismic Detection in the Aleutian Island Arc*, J. Geophys. Res. *88*, 5056–5064.

HARDEBECK, J.L. and HAUKSSON, E. (2001), *Crustal Stress Field in Southern California and its Implications for Fault Mechanics*, J. Geophys. Res. *106*, 21,859–21,882.

HAUKSSON, E. (1994), *State of Stress from Focal Mechanisms before and after the 1992 Landers Earthquake Sequence*, Bull. Seismol. Soc. Am. *84*, 917–934.

HAUKSSON, E. (2000), *Crustal Structure and Seismicity Distribution Adjacent to the Pacific and North America Plate Boundary in Southern California*, J. Geophys. Res. *105*, 13,875–13,903.

HERNANDEZ, B., COTTON, F., and CAMPILLO, M. (1999), *Contribution of Radar Interferometry to a Two-step Inversion of the Kinematic Process of the 1992 Landers Earthquake*, J. Geophys. Res. *104*, 13,083–13,099.

KILB, D., GOMBERG, J., and BODIN, P. (2000), *Triggering of Earthquake Aftershocks by Dynamic Stresses*, Nature *408*, 570–574.

KING, G.C.P., STEIN, R.S., and LIN, J. (1994), *Static Stress Changes and the Triggering of Earthquakes*, Bull. Seismol. Soc. Am. *84*, 935–953.

MALLMAN, E.P. and ZOBACK, M.D. (2003), *Using Seismicity Rates to Assess Coulomb Stress Transfer Models*, EOS Trans. AGU *84(46)*, Fall Meet. Suppl., Abstract S32F–03.

MARONE, C. (2000), *Earthquake Science: Shaking Faults Loose*, Nature *408*, 533–535.

MARSAN, D. (2003), *Triggering of Seismicity at Short Timescales Following Californian Earthquakes*, J. Geophys. Res. *108*, 2266.

MATTHEWS, M.V. and REASENBERG, P.A. (1988), *Statistical Methods for Investigating Quiescence and other Temporal Seismicity Patterns*, Pure Appl. Geophys. *126*, 357–372.

MCCLOSKEY, J., NALBANT, S.S., STEACY, S., NOSTRO, C., SCOTTI, O., and BAUMONT, D. (2003), *Structural Constraints on the Spatial Distribution of Aftershocks*, Geophys. Res. Lett. *30*, 1610.

OGATA, Y. and SHIMAZAKI, K. (1984), *Transition from Aftershock to Normal Activity: The 1965 Rat Islands Earthquake Aftershock Sequence*, Bull. Seismol. Soc. Am. *74*, 1757–1765.

OGATA, Y. (1988), *Statistical Models for Earthquake Occurrences and Residual Analysis for Point Processes*, J. Am. Stat. Ass. *83*, 9–27.

OGATA, Y. (1992), *Detection of Precursory Relative Quiescence before Great Earthquakes through a Statistical Model*, J. Geophys. Res. *97*, 19,845–19,871.

OGATA, Y. (1999), *Seismicity Analysis through Point-process Modeling: A Review*, Pure Appl. Geophys. *155*, 471–507.

OGATA, Y., JONES, L.M. and TODA, S. (2003), *When and Where the Aftershock Activity was Depressed: Contrasting Decay Patterns of the Proximate Large Earthquakes in Southern California*, J. Geophys. Res. *108*, 2318.

REASENBERG, P.A. (1985), *Second-order Moment of Central California Seismicity, 1969–1982*, J. Geophys. Res. *90*, 5479–5495.

REASENBERG, P.A. and MATTHEWS, M.V. (1988), *Precursory Seismic Quiescence: A Preliminary Assessment of the Hypothesis*, Pure Appl. Geophys. *126*, 373–406.

REASENBERG, P.A. and SIMPSON, R.W. (1992), *Response of Regional Seismicity to the Static Stress Change Produced by the Loma Prieta Earthquake*, Science *255*, 1687–1690.

SHIMIZU, R. and YUASA, M. (1984), *Normal Approximation for Asymmetric Distributions*, Proc. Inst. Stat. Math. *32*, 141–158.

STEIN, R.S., KING, G.C.P., and LIN, J. (1992), *Change in Failure Stress on the Southern San-Andreas Fault System Caused by the 1992 Magnitude = 7.4 Landers Earthquake*, Science *258*, 1328–1332.

TODA, S., STEIN, R.S., REASENBERG, P.A., DIETERICH, J.H., and YOSHIDA, A. (1998), *Stress Transferred by the 1995 $M_w = 6.9$ Kobe, Japan, Shock: Effect on Aftershocks and Future Earthquake Probabilities*, J. Geophys. Res. *103*, 24543–24565.

TODA, S., STEIN, R.S., and TAKESHI, S. (2002), *Evidence from the AD 2000 Izu Islands Earthquake Swarm that Stressing Rate Governs Seismicity*, Nature *419*, 58–61.

TODA, S. and STEIN, R. (2003), *Toggling of Seismicity by the 1997 Kagoshima Earthquake Couplet: A Demonstration of Time-dependent Stress Transfer*, J. Geophys. Res. *108*, 2567.

UTSU, T. (1961), *A Statistical Study on the Occurrence of Aftershocks*, Geophys. Mag. *30*, 521–605.

UTSU, T. (1970), *Aftershocks and Earthquake Statistics (II)- Further Investigation of Aftershocks and other Earthquake Sequences Based on a New Classification of Earthquake Sequences*, J. Fac. Sci., Hokkaido University, Ser. VII, *3*, 197–266.

VERE-JONES, D., *Statistical Methods for the Description and Display of Earthquake Catalogs*. In *Statistics in the Environmental and Earth Sciences* (eds. Walden A. T. and Guthorp P.) (Edward Arnold Publisher 1992), pp. 220–246.

VOISIN, C., COTTON, F., and DI CARLI, S. (2004), *A Unified Model for Dynamic and Static Stress Triggering of Aftershocks, Antishocks, Remote Seismicity, Creep Events and Multisegmented Supture*, J. Geophys. Res. *109*, 06304.

VOISIN, C., CAMPILLO, M., IONESCU, I., COTTON, F., and SCOTTI, O. (2000), *Dynamic vs. Static Stress Triggering and Friction Parameters: Inferences from the November 23, 1980, Irpinia Earthquake*, J. Geophys. Res. *105*, 21,647–21,659.

WALD, D.J. and HEATON, T.H. (1994), *Spatial and Temporal Distribution of Slip for the 1992 Landers, California Earthquake*, Bull. Seism. Soc. Am. *84*, 668–691.

WOESSNER, J., HAUKSSON, E., WIEMER, S., and NEUKOMM, S. (2004), *The 1997 Kagoshima (Japan) Earthquake Doublet: A Quantitative Analysis of Aftershock Rate Changes*, Geophys. Res. Lett. *31*, 03605, doi:10.1029/2003GL018858.

WYSS, M. and WIEMER, S. (2000), *Change in the Probability for Earthquakes in Southern California due to the Landers Magnitude 7.3 Earthquake*, Science *290*, 1334–1338.

ZHUANG, J., OGATA, Y., and VERE-JONES, D. (2002), *Stochastic Declustering of Space-time Earthquake Occurrences*, J. Am. Stat. Assoc. *97*, 369–380.

(Received February 13, 2004, accepted July 30, 2004)

To access this journal online:
http://www.birkhauser.ch